AN ABSTRACT OF THE THESIS OF

Richard John Meier for the degree of Master of Science in

Electrical and Computer Engineering presented on June 12, 2015.

Title: Toward Automated Decision-Making in Power Systems Wide-Area Protection

Abstract approved: ____

Eduardo J. Cotilla-Sanchez

In recent years there have been many improvements in the reliability of critical infrastructure systems. Despite these improvements and despite targeted efforts to improve the operation and control of the electric grid, the power systems industry has seen relatively small advances in this regard. For instance, today's power system is increasingly affected by power quality deficiencies, a high number of local and regional contingencies, malfunctions in equipment, and severe emergency cascading outages. This research proposes an automated decision-making framework for protecting the power network from such events. Because automated responses to emergency situations are dependent on an observable system, this work first proposes a synchrophasor data analysis methodology that leverages statistical correlation techniques in order to identify data inconsistencies, power system events, and malicious cyber-attacks. The results of this preliminary identification method show that decorrelation of PMU data streams around a network may be a valid means of initiating further automated protection and control.

Assuming a robust and automated wide-area monitoring methodology, this research also proposes a novel, algorithmic approach to selecting Remedial Action Schemes (RASs) in order to optimize the operation of the power network during and after a contingency. Specifically, this work implements an algorithm called policy-switching to consolidate traditional load shedding and islanding schemes into a robust protection policy. In order

to model and simulate the functionality of the proposed power systems protection algorithm, this work conducts Monte-Carlo, time-domain simulations using Siemens PSS/E. The algorithm is tested with experiments on the IEEE 39-bus model as well as the 2383-bus Polish model, demonstrating that this protection framework achieves optimal power system performance via automated decision-making.

Toward Automated Decision-Making in Power Systems Wide-Area Protection

by
Richard John Meier

A THESIS

submitted to

Oregon State University

in partial fulfillment of
the requirements for the
degree of

Master of Science

Presented June 12, 2015
Commencement June 2015

Master of Science thesis of Richard John Meier presented on June 12, 2015

APPROVED:

Major Professor, representing Electrical and Computer Engineering

Director of the School of Electrical Engineering and Computer Science

Dean of the Graduate School

I understand that my thesis will become part of the permanent collection of Oregon State University libraries. My signature below authorizes release of my thesis to any reader upon request.

Richard John Meier, Author

ACKNOWLEDGEMENTS

Academic

Throughout my academic career here at Oregon State University I have been supported by numerous faculty, staff, and fellow students. I am truly grateful to each and every person that I have had the pleasure to learn from, work for, collaborate with, and mentor. The school of Electrical Engineering and Computer Science here at OSU, and the amazing people that define it, have become a family to me and will always be a part of my success as both an undergraduate and graduate as well as future successes as a professional.

Specifically, and most notably, I would like to thank Dr. Eduardo Cotilla-Sanchez for believing in me and taking me on as one of his first graduate students. His wealth of support both academically and personally, his deep understanding of this challenging subject and willingness to share that knowledge, and his reliably composed, organized, compassionate, and professional nature were all key aspects to my success over the past years. Without his mentorship I would not be where I am. Others that have been important factors in my success as an electrical and computer engineering graduate student include Dr. Alan Fern, Dr. Robert Bass, Dr. JiaJia Song, Mr. Ben McCamish, and Mr. Jesse Hostetler. Thank you all for your wealth of knowledge, time, patience, and support during my time here as a graduate student. Finally, I would like to extend thanks to all the wonderfully talented, intelligent, and kind-hearted people in the Energy Systems group – the remaining professors Dr. Annette von Jouanne, Dr. Ted Brekken, and Dr. Julia Zhang – as well as each and every graduate student in this outstanding group of scholars. You have all been sources of friendship, inspiration, and thought-provoking conversation/collaboration.

Without the academic support of all of the aforementioned, this research would not have been possible. I am indebted to each and every one of you.

Personal

Though very personal to me, my faith has played a pivotal role in my academic, personal, and professional accomplishments. For that reason, I would like to start by thanking God for blessing me with courage, determination, and a supportive group of family, friends, mentors, and colleagues.

To my parents Jack and Danielle – your love and constant belief in me have been key to my success. You both have given me so much to be thankful for, and thanks seems not enough for your unwavering support throughout my academic career. I love you both and thank you for all you have done, and all you continue to do.

To my sister Jessie – your love, friendship, confidence, and advice has always been so appreciated. You have given me more than you will ever know by constantly being my biggest cheerleader. I have always been able to rely on you, and without that, I know for a fact that this work and my successes would have never been possible. From the bottom of my heart I love you and thank you.

To all my family and friends – you know who you are – thank you all for always believing in me.

TABLE OF CONTENTS

TABLE OF CONTENTS (Continued)

LIST OF FIGURES

LIST OF TABLES

Toward Automated Decision-Making in Power Systems Wide-Area Protection

1 INTRODUCTION

1.1 Motivation

Throughout the past decade, and into the next decade, the electric power system has, and will continue to see, changing paradigms in how electrical energy is generated, controlled, and consumed. The importance of the grid and the power and services that it provides will continue to make the maintenance, operation, control, and protection, of energy infrastructure and technologies a critical area of research and innovation.

The shift in operation and consumption in the electric network can be seen on many fronts. In the production of power there is a significant push for adopting renewable sources of power in an effort to reduce dependency on fossil fuels and cut carbon emissions. The U.S. President's Climate Action Plan calls for cutting carbon emissions by doubling the 2012 renewable power capacity by 2020 [4]. This is seen implemented at the macro-scale and micro-scale with construction of both large renewable generation farms as well as small distributed energy resources at the community or residential level [5]. Not only does this plan put significant pressure on power producers, but it also calls for "expanding and modernizing the electric grid" in order to handle the changes in the generation portfolio [4].

In control and delivery of electrical power there are new concerns with increased congestion as well as variability in both generation and load. This is especially evident with aging infrastructure needing to support more demand and more penetration of nondispatchable generation sources. Due to these increased constraints, exogenous events continue to result in more complex contingency situations thus increasing the likelihood of widespread outages at both the transmission and distribution levels. Examples of harmful exogenous events might include extreme variability in load or generation, machine or component failure, adverse weather, and even acts of terrorism [6]. In addition to these failures, there are intrinsic failures that include operator error, improper device settings or maintenance, and miscalculation of generation or load balance. Though power systems engineers and scientists are continually striving to find methods that mitigate the effects of these system perturbations, it is evident that these outages are still too frequent [7].

Finally on the customer-side, significant changes have occurred in load profiles due to transportation electrification, effects of weather and temperature on heating/cooling load, and a shift toward the use of power electronics for control of traditionally synchronous machinery [8, 9]. There has also been a large shift away from traditional manufacturing facilities towards consumer-electronics fabrication plants, and large data centers. This shift has seen not only more demand for reliable electric power, but also for higher quality electric power. In order to reliably provide power to this new type of demand, power engineers are striving to increase the observability and controllability of the grid. At the transmission and distribution level, synchrophasors or phasor measurement units (PMUs) are improving the observability and state estimation capability of the grid, and at the residential/commercial level, building automation and data collection are enabling better understanding of load composition and implementation of programs such as demand response that facilitate more advanced controls.

Electricity is a key aspect to the long-term success of our economic, societal, industrial, and political institutions. Therefore, it is paramount to continue to move towards a more automated operational and decision-making framework that leverages modern technologies in order to provide resilient, safe, efficient, clean, and reliable electric power.

1.2 Research Contribution

The following research will highlight the work done in order to improve the automation capabilities of wide-area controls and protection of the power system. With the previously discussed motivational factors in place (Section 1.1), and the understanding that power system technology must continue to advance alongside other related disciplines, it is the belief of the author that the natural delineation of the power system will be towards a system aided by automated decision-making algorithms. It is not the scope of this work to argue the extent or depth of this transition, but rather to highlight the work done toward leveraging synchrophasor technology and data processing [10, 11] for improved wide-area monitoring, state estimation, and data collection. Further, under the assumption of the necessary data inputs from high-fidelity PMU data, this research focuses on the development of an artificial intelligence based approach to studying and preventing large cascading outages, grid voltage collapse, and other contingency propagation mechanisms [12]. This work, and other similar works, support the advancement of the electric power system's infrastructure through intelligent technologies that further the vision of a vertically-integrated, automated (or semi-automated) framework for the operation of the electric network. A simple block-diagram of this system can be seen in Figure 1.1. Further details about the goals of this research, and how it aligns with history, other studies, and current research toward related frameworks, will be covered next in Sections 1.3 and 1.4.

1.3 Wide-Area Monitoring

Although the primary focus of this research is to improve wide-area controls and decision-making, the author recognizes that this is only possible when coupled with a robust input stream of data that characterizes the state of the network. Without high-

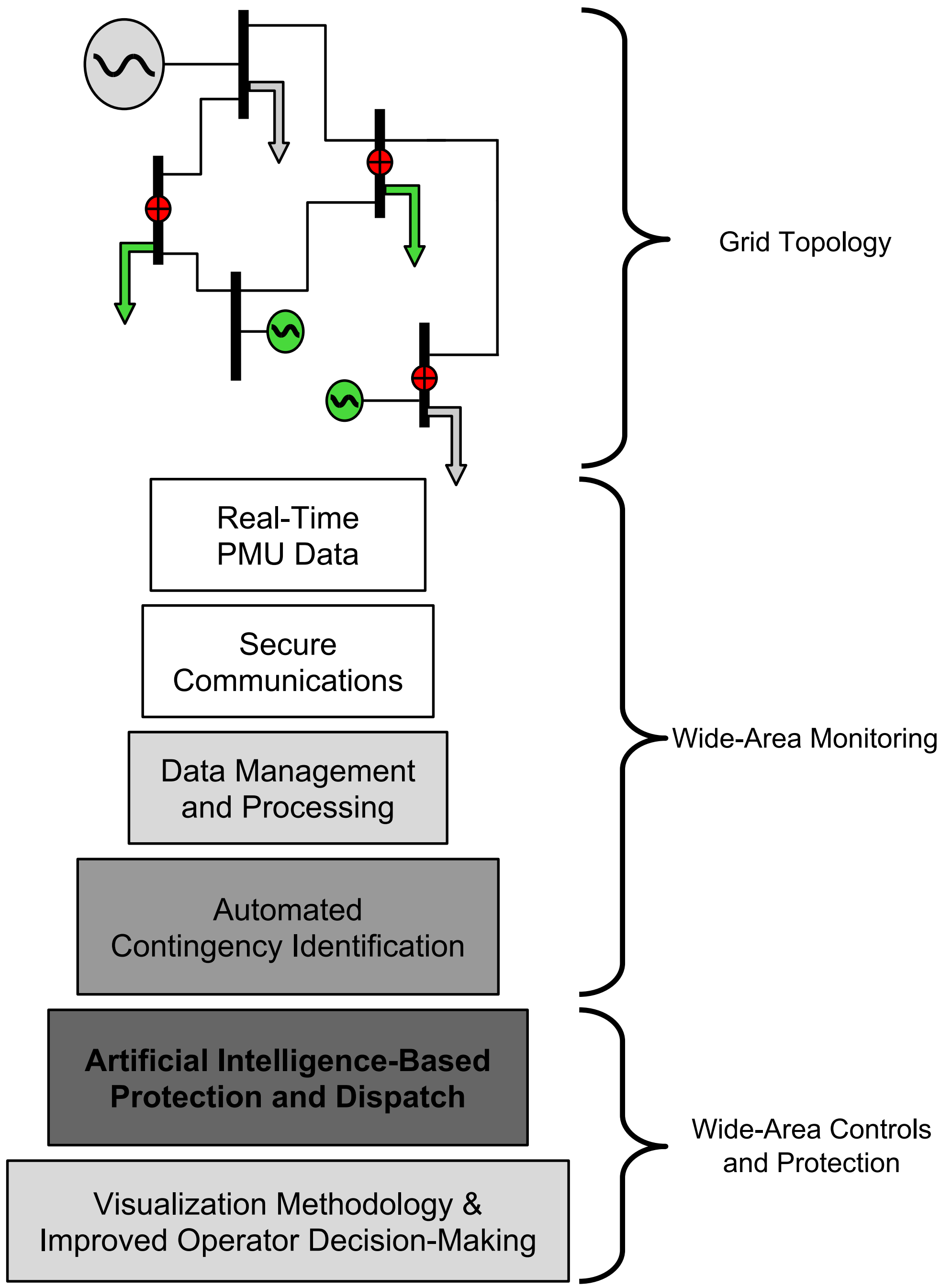

FIGURE 1.1: Block diagram of the proposed future grid operational framework. Block shading indicates level of contribution of this research.

fidelity, wide-area monitoring systems (WAMS), advanced methods of control are near impossible. For this reason, this research will begin by introducing some preliminary work done to automate WAMS using PMUs.

There is a significant push to improve the reliability of the grid by increasing the amount of operational data that provides insight into the state of the power system. As Horowitz, *et al.* discuss, there are multiple aspects to achieving the level of knowledge and control necessary to keep one of the world's greatest engineering feats stable and operational [13]. A few notable characteristics that apply to this research are: improved and accurate sensing and measurement capability, advanced control methods, and decision support. To this end PMUs seem the most likely solution to the sensing and measuring aspect. The massive amounts of data acquired by this technology should be leveraged to optimize the operation of electric power grids. The U.S. Department of Energy and other publicly and privately invested organizations have been working on installing and using these devices across the nation's grid [14, 15] dramatically increasing the amount of available data over recent years.

1.3.1 Current Research on Improving PMU Data Usage

Other works have addressed the possibility of obtaining erroneous data from PMUs and subsequently using this data for wide area monitoring and decision making. This is a significant issue, and both [16] and [17] develop algorithms for analyzing and improving data integrity during fault or transient situations. Even in static – or nominal – operation, data integrity [18] and cybersecurity [19] are some of the most common problems that current research thrusts are trying to address. The methodology for analyzing PMU data presented here strives to make advancements toward these ends.

Not only is synchrophasor data analysis a current research trend, but recent works are also still investigating the different engineering applications that PMUs may have in monitoring the grid. Some efforts have emphasized using PMU data to monitor critical power paths [20], identify transmission line fault locations [21], isolate and mitigate low-frequency zonal oscillations [22], and predict critical slowing down of the system [23]. Further, [24] has stressed that synchrophasors are indeed a valid solution for wide area monitoring systems (WAMS) and state estimation – although there are still many challenges to address.

1.3.2 History and Motivation for PMUs in Energy Management Systems

Traditionally, the SCADA framework has been used to measure important power system quantities (e.g., voltage, current, and frequency) needed for state estimation [25]. The majority of Energy Management Systems (EMSs) are based on SCADA applications. SCADA has proven to be an important piece of sensing, observing, and controlling the state of the power system; despite its development in the mid-1980s, the PMU did not become a significant factor in monitoring and EMS applications until after the North American Blackout of 2003 [14, 26]. Even today, the use of real-time synchrophasor data is an active area of research and development.

There has been a shift toward the use of PMUs to aid state estimation primarily due to their ability to capture transients and other dynamic system states [27]. The high-fidelity data streams allow forecasting of states using a dynamic state estimator which was previously impossible to obtain with traditional static state estimation – on which SCADA EMSs are based. Figures 1.2 and 1.3 depict a comparison of power system frequency data obtained with the SCADA system and a PMU of an event occurring on February 7, 2010 [1]. As seen, this NERC report shows a 10 minute window of SCADA data that does not do an adequate job of capturing the transient excursion of a frequency signal due to a specific power system event. By observing the PMU network over a smaller time window (44 seconds) the report details how the PMU is able to accurately portray the oscillations and instantaneous magnitude of the event.

FIGURE 1.2: 10 minute SCADA window depicting a power system event on February 7, 2010 [1].

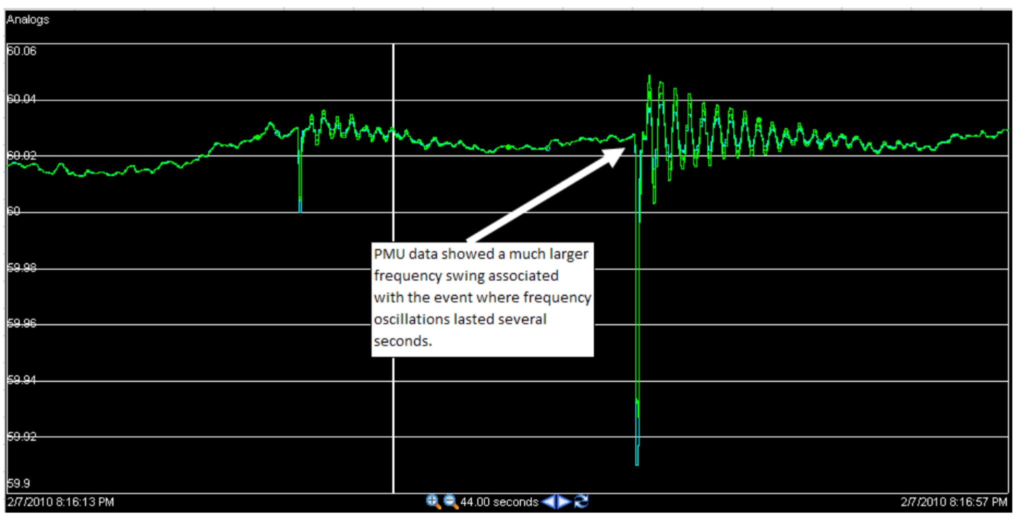

FIGURE 1.3: Power system event from Fig. 1.2 observed with a PMU data stream. Higher fidelity data allows a more accurate portrayal of the state of the system [1].

1.4 Wide-Area Protection and Controls

The primary aim of this research is to develop a wide-area control strategy for preventing large blackouts and cascading events. Typically, utility operators manually program Remedial Action Schemes (RASs)[1] in order to prevent large voltage instabilities or power delivery and reliability issues that are caused by extreme contingency situations. The remainder of this section covers the current research in RAS design (1.4.1), followed by the implementation of RASs and the contribution of this work to that end (1.4.2).

1.4.1 Remedial Action Schema

The breadth of Remedial Action Schemes (RASs) is vast and continually expanding. Traditionally, two protection actions have proven to be highly effective as part of a RAS - namely load shedding and islanding. Load shedding has many design implementations ranging from homogeneous, naive techniques [28, 29] to highly complex and adaptive [30–32]. Load shedding is a powerful scheme because it fundamentally seeks to optimize the power flow so that load and generation match precisely. Also, depending on its complexity, the computation time is often small enough to merit on-line operation. Islanding, on the other hand, is a relatively new method for protection. Its main purpose is to isolate functional sections of the power system so that a contingency does not cascade and become more severe. Some studies have been done with regard to the effectiveness of islanding on both micro and macro scale grid topologies [33] [34]. Others have started to consider the effects of having distributed generation (DG) sources contained within islands [35]. Despite the many factors that influence the use of islanding, it is largely agreed upon that this protection method is useful for improving the operation of a power system in some contingency situations [36]. Typically islanding policies have been determined offline by simulating a large set of different contingencies and finding sections of the grid that can continue to operate independently of adjacent grid infrastructure. Reference [36] also proposes one of the first on-line islanding algorithms.

[1] They are also known as Special Protection Schemes (SPS) or System Integrity Protection Schemes (SIPS).

1.4.2 RAS Implementation

Besides RAS design, there is also discussion about how to best evaluate or implement these RASs. Some research supports decentralized approaches to wide-area protection [37], while others argue that a centralized approach is best [38–40]. Some of these approaches include heuristic or monte-carlo search algorithms. Others take approaches based on topological and/or observational inputs such as electrical distance [41], frequency instability [42], or observation decision trees [43]. Still others have developed model predictive control methods on dynamic models of the power system [44]. Some classic works have used static models for study and implementation of RASs however, more recently, there is debate over whether or not the use of dc, static, or dynamic models might be more appropriate [29, 32, 45, 46].

Given the variety of load shedding and islanding approaches, along with their various combinations, the number of possible RAS policies is vast. Unfortunately, during emergency situations it is difficult to determine how to choose and implement a policy that will optimally improve network operation after a contingency. A contribution of this work is to provide a novel approach to selecting such RAS policies in a manner that maintains strong performance guarantees. Specifically, this work introduces the framework of policy switching. Policy switching is an algorithmic approach to selecting and executing the policy that exhibits the best performance according to Monte-Carlo simulation techniques [47]. As time progresses, this approach may switch between multiple policies, depending on the specific way that the grid system evolves. This methodology has been used in machine learning and artificial intelligence spheres to improve the outcomes of multiple control problems ranging from real-time strategy (RTS) games to computer networking. Grid protections provide similar control issues in that there is a wide breadth of RAS policies to choose from. Ideally, the optimal solution will be found in an automated and real-time manner. The background and methodology of this work will be further introduced in Sections 2.4 and 3.2.

1.5 Organization of this Thesis

The following work is organized around two main research thrusts. First, the automated wide-area monitoring research involves the study of real-world synchrophasor data from the Bonneville Power Administration (BPA) 500kV transmission system. Second, a novel wide-area protection methodology for power systems is developed using approaches adapted from artificial intelligence and automated planning theory. Chapter 2 will introduce the fundamental technical background needed in order to understand the development of these two decision-making methodologies. Next, Chapter 3 will explain the features of this research and the set-up of the experimentation. This will begin with the synchrophasor correlation method in Section 3.1, followed by the automated planning-based method in Section 3.2. Chapter 4 will, similarly, be split into the two primary research topics. Section 4.1 will cover the findings related to correlation and its ability to distinguish data issues, power system contingencies, and cyber attacks. Section 4.2 will highlight the findings of using policy switching, via power system time-domain dynamic modeling, as a tool to determine optimal RASs. Finally Chapter 5 will provide some additional discussion and suggest some future work for the continued development of this methodology.

2 BACKGROUND

2.1 Synchrophasor Technology

2.1.1 Phasor Measurement Units (PMUs)

PMUs measure the instantaneous voltage, current, and frequency at specific locations in a power system (usually at transmission substations) [14] by generating phasor measurements. Each phasor measurement is time-stamped via Global Positioning System (GPS) and because it is time-synchronized, it is called a synchrophasor. As a result, PMUs in different locations can be synchronized and time-aligned, then integrated to provide a precise, comprehensive view of an entire region or interconnection. The data conversion process from a sinusoidal waveform to its phasor representation, as logged by a PMU, is shown in Fig. 2.1.

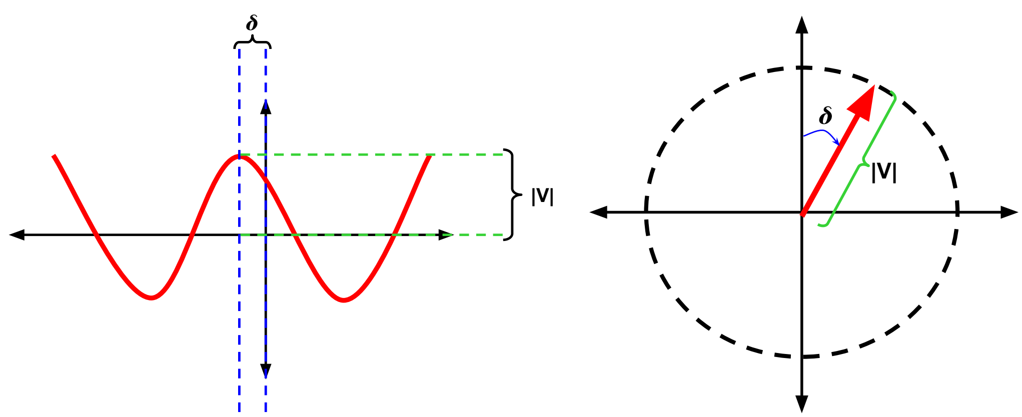

(a) Voltage sinusoid. (b) Voltage phasor.

FIGURE 2.1: PMU conversion of sinusoids to phasors.

2.1.2 SCADA vs Synchrophasors

According to NERC and IEEE standards [1,48,49], PMUs are normally sampled at 30 Hz, however, this sampling rate can go up to 60 or 120 Hz. The 60 Hz measurement is becoming more common for large regional transmission organizations (RTOs) and large balancing authorities (BAs). Compared to conventional monitoring technologies such as SCADA – which only measures once every two to four seconds – PMU technology represents a significant increase in data gathering. SCADA monitoring systems are starting to become less reliable for effectively creating accurate state estimations during emergency events because SCADA data do not track dynamic events on the grid. Current SCADA systems do not monitor key indicators such as phase angles, and SCADA data are also not consistently time-synchronized and time-aligned, nor are those data capable of easily being shared widely across the grid.

2.1.3 The Phasor Data Concentrator

Since each PMU operates in a decentralized manner, the PMU data streams must be coalesced to a single point. The gathering of individual PMU data streams occurs at a device[2] called the Phasor Data Concentrator (PDC). The PDC is typically the hub for PMU data communication, and according to [1] there are different types of PDCs based on the number of PMUs it can multiplex as well as the location that the PDC is placed. Figure 2.2 below shows a visual depiction of the different PDCs scaled by their location and the number of supported PMU streams [1].

[2]PDCs can also be completely software-based.

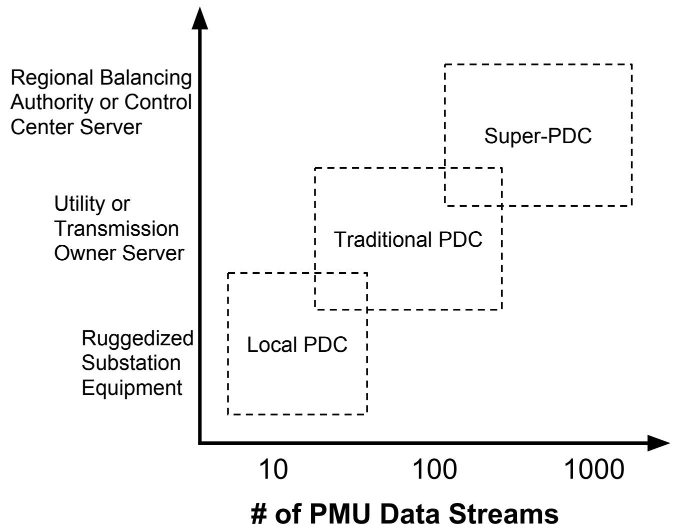

FIGURE 2.2: PMU data aggregation into PDC devices [1].

2.2 Static and Dynamic Modeling of Power System Operation

In its most reduced form, the power system can be considered a system of nonlinear algebraic and differential equations. In dynamic representations, or models, of a power network, both algebraic and differential equations are used to calculate power flows, determine machine operation, model protection devices, and ultimately determine the dynamic stability of the system. In many scenarios, however, power system operators are able to assume small perturbations to this dynamic system, and therefore simplify equations with static power flow calculations neglecting the transient operation of machines and loads because of the assumption of near nominal performance. In other engineering applications, a dc approximation to the static ac power flow can be used where further assumptions about reactive power, bus angles, and bus voltages are made.

The following subsections highlight some of the fundamental mathematics behind power system modeling. In the case of this research, dynamic power system modeling was required, because of the nature of severe contingencies and their transient and/or oscillatory effects on the operation of the power network. Studying these effects using simple dc or static ac modeling approaches would not allow for adequate evaluation of the RAS implementation methodology. Mainly, this is because RAS implementation is meant for emergency situations which typically deviate far from nominal operation as the network approaches voltage collapse – at this point, static ac modeling breaks down in its ability to accurately represent the network.

2.2.1 Static AC Power Flow

The solution for the ac power flow is based off of Kirchoff's Nodal Analysis – a system of equations in the form:

$$\mathbf{I} = \mathbf{Y_{bus}} \cdot \mathbf{V} \tag{2.1}$$

where $\mathbf{I}$ is a vector of complex current injections, $\mathbf{Y_{bus}}$ is the admittance matrix based on the topology of an N-bus system, and $\mathbf{V}$ is the vector of complex voltages at each of the N buses.

Choosing a single bus in the N bus network, say bus k, equation 2.1 becomes:

$$I_k = \sum_{n=1}^{N} Y_{kn} V_n \tag{2.2}$$

Given that apparent power at bus k is:

$$S_k = P_k + \jmath Q_k = V_k \cdot I_k^* \tag{2.3}$$

It is possible to obtain a combination of equation 2.2 and 2.3 as follows:

$$P_k + \jmath Q_k = V_k \left(\sum_{n=1}^{N} Y_{kn} V_n \right)^* \tag{2.4}$$

Converting Y_{kn} to its rectangular values $(G_{kn} + \jmath B_{kn})$, and incorporating the phase angle difference (δ) between bus k and bus n, equation 2.4 becomes the power flow equations (power injection at bus k):

$$P_k = V_k \sum_{n=1}^{N} V_n \left(G_{kn} \cos(\delta_k - \delta_n) + B_{kn} \sin(\delta_k - \delta_n) \right) \tag{2.5}$$

$$Q_k = V_k \sum_{n=1}^{N} V_n \left(G_{kn} \sin(\delta_k - \delta_n) - B_{kn} \cos(\delta_k - \delta_n) \right) \tag{2.6}$$

This system of equations for each bus in the system characterizes the power flow of the network. These equations are then solved by iterative means such as the Gauss-Seidel or Newton-Raphson algorithms [50].

2.2.2 The DC Approximation

In modeling of the power system it is sometimes common to see further simplification of the power flow equations 2.5 and 2.6. This method for approximating power flow is an effort to speed up calculation, and get a rough estimate of active power flow around the network during nominal operation. The three main simplifications to achieve the dc power flow include:

1. The vector of bus voltages is equal to 1 per unit:
   $\mathbf{V} = \mathbf{1}\text{pu}$
2. The phase angles between buses are assumed to be very small radian values:
   $\sin(\delta) = \delta$
3. Reactive power flow is neglected (equation 2.6 is ignored):
   $Q_k = 0$

All this results in a simple linear expression for active power flow [50]:

$$P_k = \sum_{n=1}^{N} B_{kn}(\delta_k - \delta n) \tag{2.7}$$

2.2.3 Dynamic Power Systems Modeling

Time domain dynamic simulation is another method for modeling of the electric power system. This simulation technique is, by far, the most computationally expensive and generally more complex than the static ac and dc methods explained in the previous two sections. Dynamic power system modeling is meant to provide alignment with real-world operation because it typically includes the physical and electrical constraints of generators, loads, and relays, as well as the primary controlling mechanisms for their operation. In effect, the mechanical motion and oscillation, as well as electrical transients, along with closed-loop feedback devices (like governors and exciters) that control these transients, are modeled in the differential portion of the system of equations. It is possible to now envision the power flow and power system modeling problem, generally, as the system of differential (f), algebraic (g), and discrete (h) equations in eqn. 2.8:

$$\begin{cases} \dot{\mathbf{x}} = f(t, \mathbf{x}(t), \mathbf{y}(t), \mathbf{z}(t)) \\ \mathbf{0} = g(t, \mathbf{x}(t), \mathbf{y}(t), \mathbf{z}(t)) \\ \varepsilon > h(t, \mathbf{x}(t), \mathbf{y}(t), \mathbf{z}(t)) \end{cases} \tag{2.8}$$

where the $\mathbf{x}$, $\mathbf{y}$, and $\mathbf{z}$ are variables that are all vectors of parameters representing various devices in the power system model. Specifically, $\mathbf{x}$ contains parameters representing devices that have intrinsic dynamic (transient) behavior (such as machines, loads, governors, and exciters). $\mathbf{y}$ represents devices that have algebraic relationships and are typically associated with those variables that determine the power flow. $\mathbf{z}$ is another vector of parameters representing devices that act discretely (such as transmission line relays). Each parameter in $\mathbf{z}$ (z_i) is associated with a threshold value in the vector ε (ε_i) where the discrete device activates when the inequality h is not satisfied. In other words, when any variable in $\mathbf{x}$, $\mathbf{y}$, or $\mathbf{z}$ violates the thresholds in ε then the corresponding discrete device will activate within the grid model [50, 51].

The coefficients and values that are found in the vector of differential variables ($\mathbf{x}$)

are determined by the models used for the power system's generators, speed governors controllers, and voltage exciter controllers. In this case, the author, limits the scope of dynamic parameters to these three devices for the sake of developing simpler, yet still realistic, transient stability models. In building the dynamic models of the power system, and in determining appropriate parameters, the PSS/e manuals [52, 53], the PowerWorld user's guide [2], Kundur's work on transient stability [51], Dr. JiaJia Song, and Dr. Eduardo Cotilla-Sanchez were all valuable resources. Three block diagrams of the general models used in this work are found in Figures 2.3, 2.4, and 2.5.

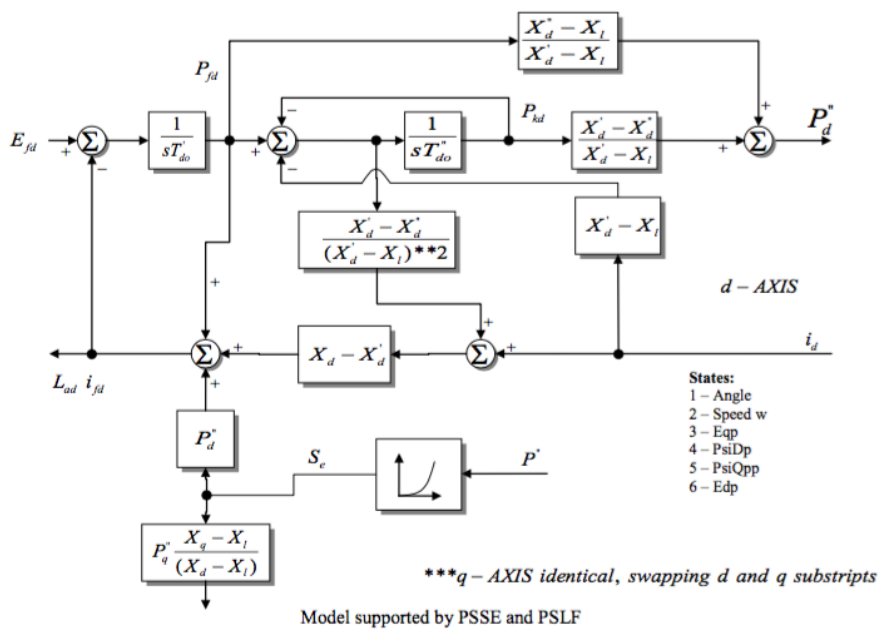

FIGURE 2.3: Block diagram model of the GENROU generating unit [2].

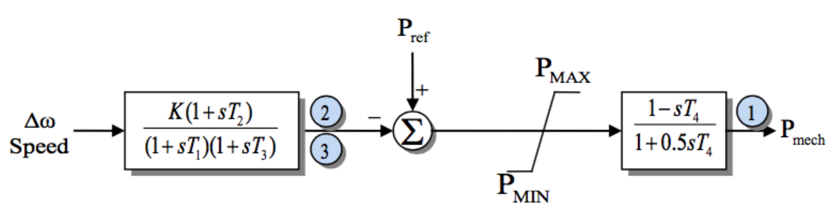

FIGURE 2.4: Block diagram model of the IEEEG2 governor unit [2].

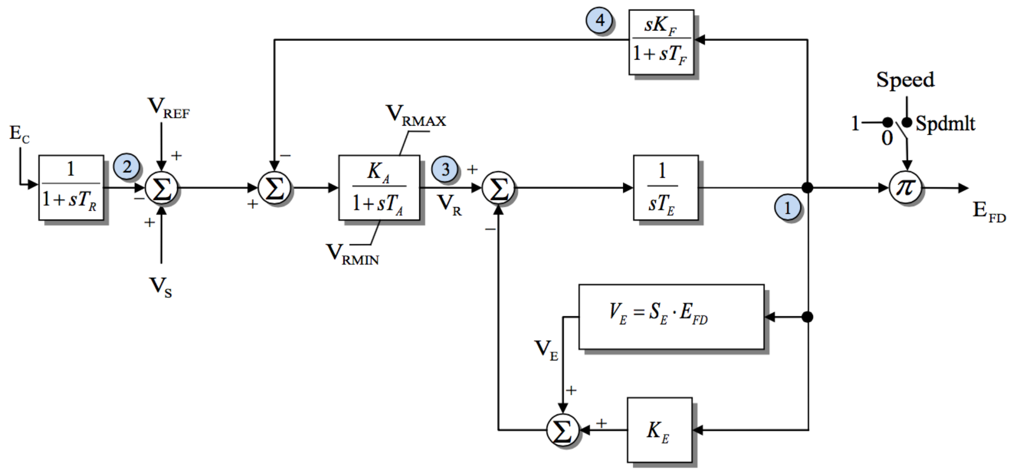

FIGURE 2.5: Block diagram model of the IEEET1 exciter unit [2].

2.3 Electrical Distance

This section introduces the concept and use of electrical distance in this research. Electrical distance is a measure of the electrical proximity of any two devices in an electrical system. In this case, the interest is in calculating the electrical distance between two arbitrary buses in an electric power network. Unlike a measure of euclidean distance, electrical distance provides a metric for understanding the coupling of two buses in a power network. Topological distance does not adequately characterize bus coherency (coupling/correlation) because this metric is fundamentally based on bus angles – which are in turn mathematically dependent on the change in power injection over time. For this reason, the formal implementation of electrical distance developed by Cotilla-Sanchez et. al. in [41], is used as one metric for portraying the results of this work. Other works have also based visualization of the power system off of electrical distance metrics such as [54]. This concept of using electrical distance as an analysis metric for power system stability as well as visualization is revisited multiple times in this work.

2.4 Automated Planning

This section introduces the fundamental framework for the primary algorithm used in this research called Policy Switching. Policy Switching falls under the category of planning algorithms which, in turn, is an active area of research in artificial intelligence (AI). One definition of AI is, as stated by Russell and Norvig, the study of rational action [55]. In the case of automated planning, that is exactly what one seeks – rational action via algorithms, heuristics, or deterministic plans to achieve the best attainable goal. The following subsections will define the necessary AI fundamentals in order to better explain the policy switching methodology in Section 3.2.3.

2.4.1 Markov Decision Processes

The control implementation introduced by this research is formalized by choosing amongst RAS policies within the framework of a Markov Decision Process (MDP) [56]. MDPs are a widely used mathematical model of controllable systems with stochastic dynamics. By modeling a control problem as an MDP, it is possible to draw on decades of research that has produced rich theory and computational solutions.

An MDP is a tuple (S, A, P, R), where S is a set of system states and A is a set of possible control actions. For example, in a power system network, each state would correspond to a possible configuration of the joint state variables in the network. Each action might correspond to the control actions available to a network operator, e.g. opening a transmission line. The third MDP component, P, is a conditional transition distribution defined such that $P(s' \mid s, a)$ gives the probability that the system will transition to state s' after action a is selected in state s. Here we assume a discrete time setting, where continuous time systems can be handled by discretizing at an appropriate time scale. Note that P defines a first-order dynamic system in the sense that the distribution over next states only depends on the current state and the selected action, rather than also depending on previous states and actions. In an electrical network, P describes network state transitions due to both electrical laws, the control actions, and random exogenous events. For example, an operator action of taking a transmission line out of service will result in transient state transitions, whereas a random (exogenous) weather event will also result in such transitions. The final MDP component, R, is a reward function that maps states to numeric rewards. In the context of power networks, $R(s)$ might measure the overall profit or quality-of-service associated with state s, noting that negative rewards can be used to model system costs. A visual representation of this explanation can be found in Fig. 2.6.

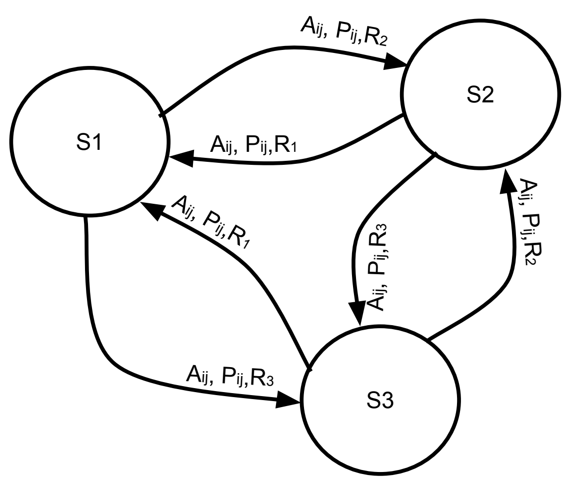

FIGURE 2.6: A visual representation of a 3-state MDP.

2.4.2 Definition of Policies

Given an MDP, the objective is to derive a controller for the system that will accumulate the largest possible long term reward by selecting appropriate actions over time. More formally, a controller for an MDP is typically referred to as a policy π which is a mapping from states to actions. Given a policy π the MDP is controlled by selecting the actions dictated by the policy in states that arise according to the MDP dynamics. Thus, a policy π defines a distribution over the possible state sequences, and in turn reward sequences, of the system over time. Intuitively, one would like to use a policy that produces sequences with large accumulated rewards, which is formalized via the concept of value functions. Each policy π is associated with a value function V^π, which is a function from states to real-numbers such that $V^\pi(s)$ measure the "quality" of π when started in state s. More formally, in this research will let $V^\pi(s)$ be the expected discounted infinite sum of rewards starting from state s given by:

$$V^\pi(s) = E\left[\sum_{t=0}^{\infty} \beta^t R(s_t)\right] \tag{2.9}$$

where $E[\cdot]$ is the expectation operator, $\beta \in (0, 1)$ is a discount factor, and s_t is a random variable denoting the state that results after starting in state s and following actions dictated by π for t steps (so $s_0 = s$). The discount factor β is included in the above expression to ensure that the infinite sum of rewards remains finite, which is accomplished by exponentially discounting future rewards at a rate of β. If a small value of β is used, then only temporally near rewards will influence the value of a policy. Rather, in practice β is often set to large values close to one to ensure that more distant rewards have significant impact on the value.

A policy π^* is said to be an optimal policy if in any state s its value $V^\pi(s)$ is at least as good as that of any other policy. A fundamental theoretical result is that every MDP has an optimal policy, though there may be multiple optimal policies (all with the same value function). Given an MDP description, it is possible to compute an optimal policy using classic algorithms such as value iteration or policy iteration [56]. Unfortunately, these algorithms are only applicable to relatively small MDPs (thousands to millions of states) and become impractical for enormous MDPs such as those that arise from large electrical networks. Further, it can be shown that computing optimal policies for such systems is formally computationally hard [57]. Thus, approximate solution approaches are generally used in such situations – namely, the algorithm policy switching. The implementation of policy switching is described in Section 3.2.3.

3 METHODOLOGY

This chapter is organized as follows. First, Section 3.1 explains the wide area monitoring approach and synchrophasor methodology. Following that, Section 3.2 will explain the methodology for the wide-area controls and protections framework.

3.1 Automated Synchrophasor Data Analysis

The goal of this Section is to describe a correlation-based method for automatically analyzing PMU data in order to differentiate between data inconsistencies and actual power system events, as well as do a preliminary study on PMU cybersecurity. The algorithm seeks to find correlation patterns among a wide variety of PMUs installed at different locations within a balancing area. A real-time playback engine of actual archived PMU data is used in order to mimic a real power system environment.

3.1.1 PDC Playback Engine

The first step in creating a real-time, data-playback engine was analyzing the characteristics of the historic datasets obtained from the Bonneville Power Administration (BPA). By understanding the file traits, recorded power system attributes, data discretization rate, and topological layout of the PMUs (depicted in Figure 3.1), a *Phasor Data Concentrator (PDC)* engine was created in software in order to mimic a real PDC data stream off of the grid.

The one-year long dataset includes information from August 2012 to August 2013. It totals 950 GB of data made up of 5 primary signals including: positive sequence voltage magnitude V_{+Mag}, positive sequence phase angle $V_{+\phi}$, negative sequence voltage magnitude V_{-Mag}, negative sequence phase angle $V_{-\phi}$, and frequency f. An additional metric, rate of change of frequency ($ROCOF$), was added by differentiating the frequency signal.

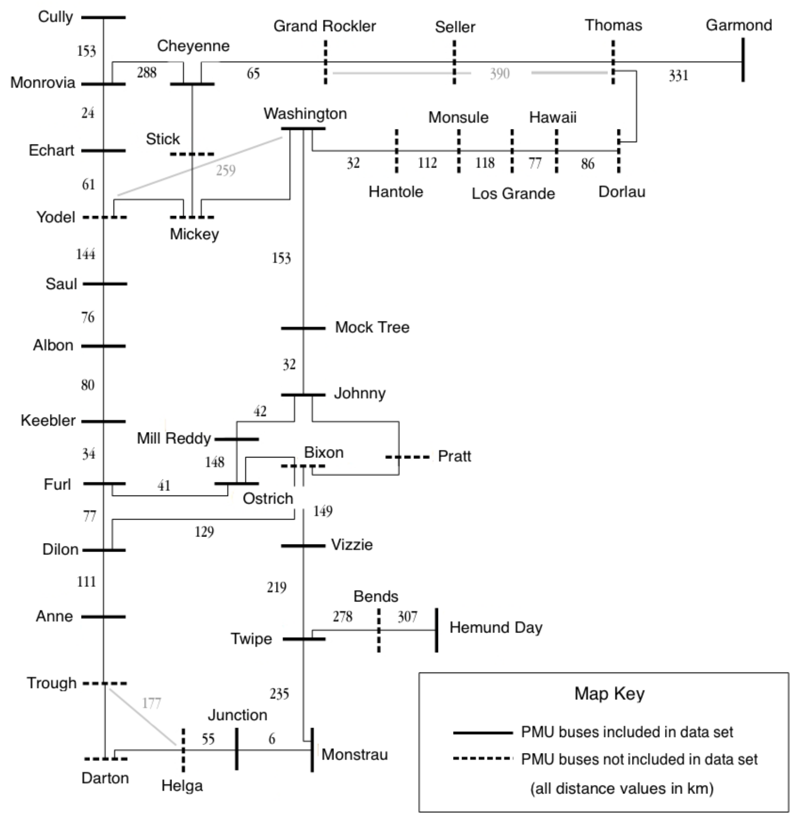

FIGURE 3.1: Anonymized topological layout of the archived data source PMU network.

Each PMU data point is represented by a *date/time* and its corresponding measurement value (in the case of positive and negative sequence voltage this value is a phasor). Each file in the provided dataset typically holds one to five minutes of data from each of the twenty PMU sites.

The goal of this research thrust is to identify the difference between data inconsistencies and power system events, and also to analyze the security of automated PMU data analysis with respect to cyber-based data-spoofing attacks. This is done by calculating and analyzing the correlation coefficient for each pair of PMU data streams (as described in Section 3.1.4). The next few subsections describe the key backend functionalities developed in this work.

3.1.2 Backend Data Management

As positive sequence voltage data is generated in the time-domain by the PDC engine, these data must be read into the working memory of the correlation algorithm. In an effort to minimize computational complexity, a custom data structure is used in order to quickly append new data, reference data already stored, and account for multiple characteristics such as time, magnitude, phase, and correlation coefficients, for each PMU. This versatile data structure is depicted in Figure 3.2.

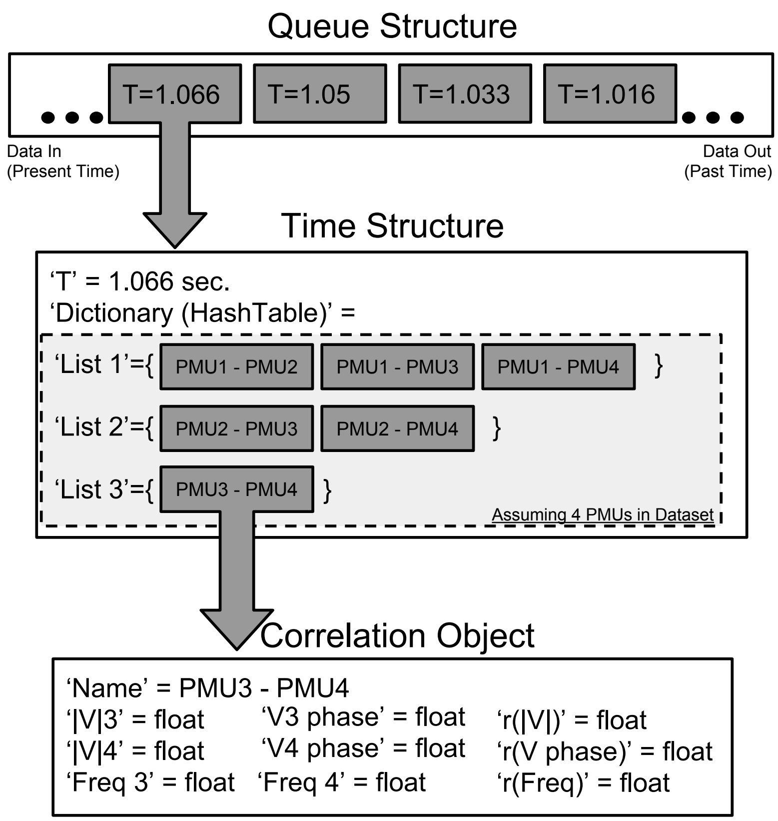

FIGURE 3.2: The three-tiered data structure used to store PMU data and correlation data.

The lowest layer of the data management system holds the actual values read in from the PDC feeder as well as the calculated correlation coefficients (referred to as "Correlation

Objects"). These Correlation Objects are dynamically created based on the number of PMUs multiplexed. The next layer of the management system is made up of Correlation Object combinations at a specific time stamp (referred to as "Time Structure"). This creates a triangular matrix of Correlation Objects that reference both a unique time as well as the PMU data and correlation value at that particular time. Finally, at the highest management level, each Time Structure is stored in a queue of dynamic length. The PMU and correlation data can be monitored in the time domain for any desired window of time. Since this data structure is a generic, user-defined object, it is possible to insert other PMU traits, correlation techniques, and flagging variables for easily analyzing PMU relationships over time – future use of this data structure is facilitated by its flexibility in holding various metrics.

3.1.3 PMU Signal-to-Noise Ratio Analysis

A signal-to-noise ratio analysis was performed on the raw PMU data fed by the PDC engine. This was useful in order to identify the most useful PMU data signals for correlation-based identification of power system events, data inconsistencies, and cyber-based spoofing attacks.

It is helpful to begin with a definition of the noise floor. In signal analysis, the noise floor of a signal is a measure of the ratio between the summation of all the intensities over the signal spectrum and the intensity of the primary signal's frequency(ies) [58]. In other words the denominator is the power contained in the primary (monitored signal), and the numerator is the summation of the remaining signal frequencies outside that of the monitored signal. There are multiple ways to calculate the SNR of a signal, this research uses the method formally outlined below:

Given a PMU signal y there will be some true component x and some noise component n where:

$$y = x + n \tag{3.1}$$

In determining the SNR we use:

$$SNR = \frac{P_x}{P_n} \tag{3.2}$$

Where the power of some arbitrary discrete time signal a with N data points is:

$$P_a = \frac{1}{N} \cdot \sum_{i=0}^{N-1} (a_i)^2 \tag{3.3}$$

Since we only have the y of the desired signal we define $\hat{x}$ and $\hat{n}$ to be the supposed true signal and noise signal respectively. So:

$$y = \hat{x} + \hat{n} \tag{3.4}$$

Where $\hat{x}$ is determined by using a two-sided gaussian estimation filter (H) on the combined signal y. H takes the following form:

$$H = \frac{1}{(a_{len(y/8)} s^{len(y/8)}) + (a_{len(y/8)-1} s^{len(y/8)-1}) + ... + a_1 s + a_0} \tag{3.5}$$

Where the coefficients of the poles are of the form:

$$a_i = \mathrm{e}^{\frac{-i^2}{2 \cdot \sigma^2}} \tag{3.6}$$

This reduces the noise signal $(\hat{n})$ calculation to a difference:

$$\hat{n} = y - \hat{x} \tag{3.7}$$

And from the equations 3.2 and 3.3, we calculate the SNR of y using:

$$SNR_y = \frac{P_{\hat{x}}}{P_{\hat{n}}} = \frac{\sum_{i=0}^{N-1} (\hat{x}_i)^2}{\sum_{i=0}^{N-1} (\hat{n}_i)^2} \tag{3.8}$$

Using Matlab we calculate the SNR for each of the 6 PMU signals (V_{+Mag}, $V_{+\phi}$, V_{-Mag}, $V_{-\phi}$, f, $ROCOF$), for the window sizes 1 sec., 2 sec., 5 sec., and 10 sec at each of the 5 electrically closest buses (Mill Reddy, Johnny, Dilon, Mock Tree, and Vizzie). An example output of using approximation theory to obtain $\hat{x}$ (filtering y by the function H

to obtain an estimation for $\hat{x}$) can be seen in Figure 3.3. This shows the original signal in red and the filtered (approximated) signal in blue. It is apparent from this visualization that the noise associated with the frequency feature is fairly low, and the SNR results obtained for each window size are seen in Fig. 3.4.

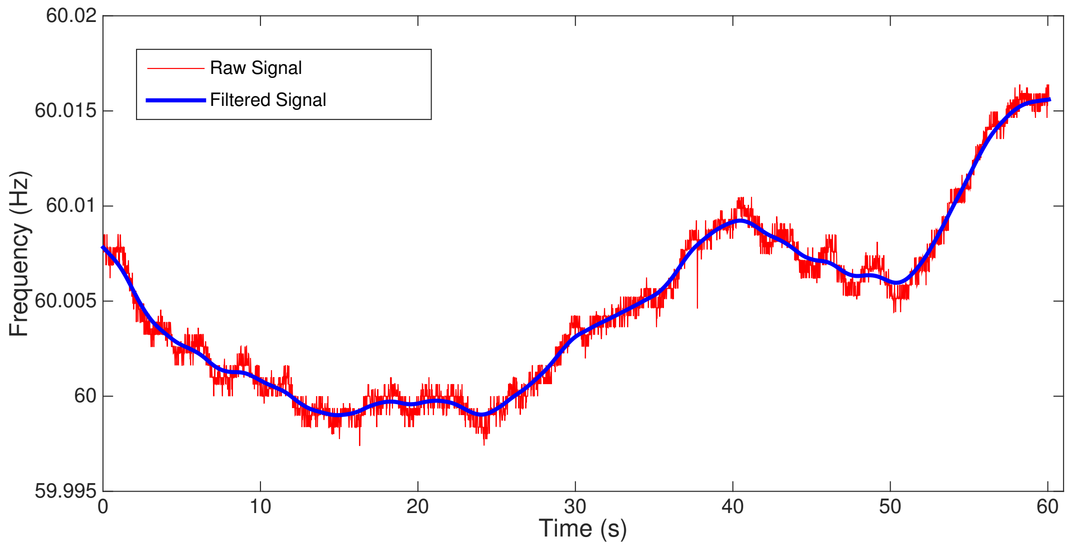

FIGURE 3.3: The Gaussian filter imposed on a sample of the frequency (f) signal.

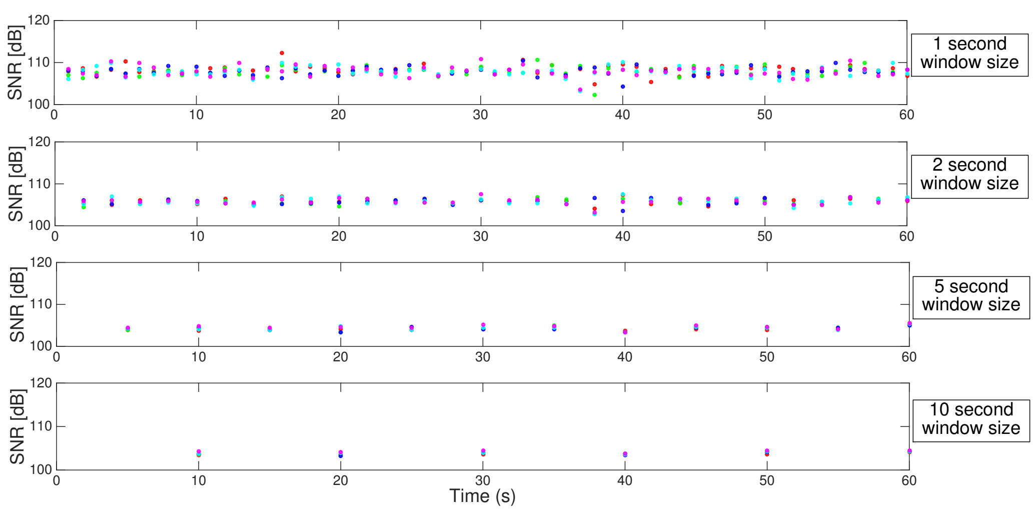

FIGURE 3.4: SNR for the frequency PMU signals over varying window sizes.

The results in Figure 3.4 show that as window size increases, the noise component increases slightly, and the spread of noise across each of the five electrically close PMUs (represented by the various colors) decreases. For each of the PMUs and window sizes the SNR is quite high suggesting that there is not a significant amount of noise contained in the frequency signal. The SNR results for every single PMU data stream are not included here, however each of the signals (except $ROCOF$) were similar in the amount of power contained in the noise – that is, the noise was not a significant component. The following research will, both for the sake of clarity and data availability, primarily use the voltage magnitude (V_{+Mag}), phase ($V_{+\phi}$), and system frequency (f) PMU components while also considering the various window sizes.

3.1.4 Correlation Approach

The premise of this research methodology is that due to the electrical cohesiveness of the power network, data at buses around the system will be linearly correlated to some non-trivial degree. This will likely differ from bus to bus, or node to node, however in the event of some data inconsistency or power system contingency, it is expected that some amount of decorrelation will occur. Hypothetically, this decorrelation will reveal patterns based on severity, location of the contingency, affected nodes, and type of contingency encountered. By using this correlation method, and by intelligently managing the archived PMU data, a preliminary attempt at automatically processing input WAMS data is developed.

Correlation is a well known mathematical and statistical method for determining the compatibility of large data sets. Specifically, the Pearson Product-Moment correlation determines how well data is linearly correlated, and has been used successfully in other graph-based problems [59, 60].

Given two independent input sets of data X and Y of length N (X and Y being either the momentary magnitude or phase data values of two PMU site readings), the Pearson correlation yields a correlation coefficient r between -1 and 1 based on the following equation:

$$r = \frac{\Sigma(XY) - \frac{\Sigma X \Sigma Y}{N}}{\sqrt{(\Sigma(X^2) - \frac{(\Sigma X)^2}{N}) \cdot (\Sigma(Y^2) - \frac{(\Sigma Y)^2}{N})}} \tag{3.9}$$

Two modifications and application-specific improvements were made to this mathematical formula. First, the algorithm was made incremental. In this way, each data point could be read in from the PDC engine and immediately incorporated into its correlation coefficient without the need to directly calculate each summation, average, and standard deviation repeatedly at each time step. This helps reduce run time.

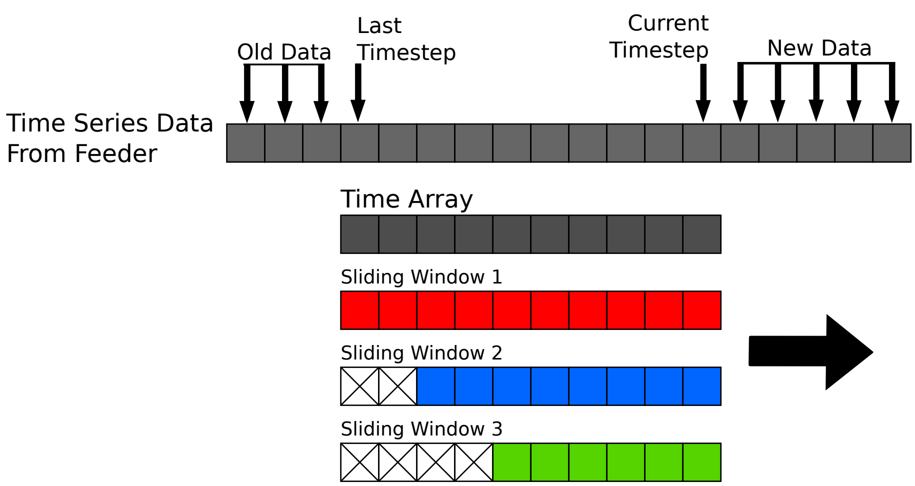

FIGURE 3.5: Sketch of the “Time Structure” data queue, and its multiple-window-size capability.

Second, the correlation algorithm was built to maintain correlation information over varying windows of time. The queue data structure maintains multiple separate pointers to end positions of each defined sliding window. This is seen in Figure 3.5. It is worth noting here that separate lists for each sliding window are *not* created. Rather, pointers in a single list are maintained to minimize memory usage, as well as minimize copies of data already managed.

The addition of this window-size feature allows for pairs of PMUs to be correlated

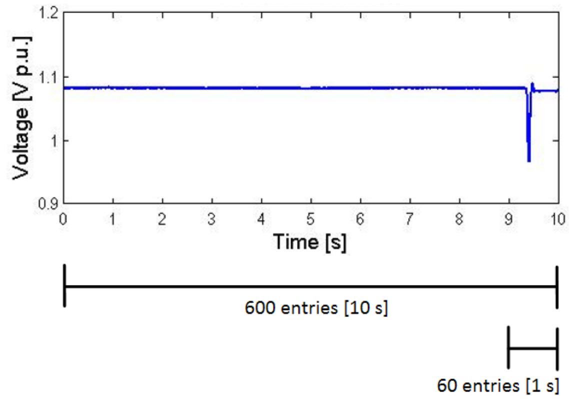

FIGURE 3.6: Voltage magnitude plot during a lightning event (large window sizes).

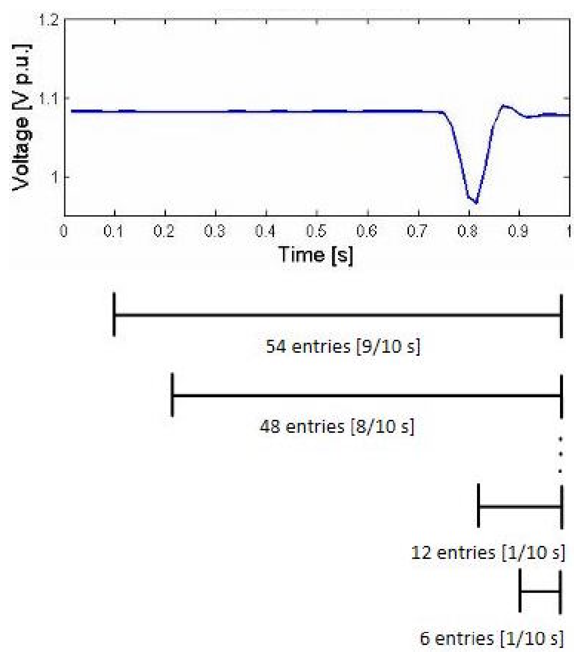

FIGURE 3.7: Voltage magnitude plot during a lightning event (small window sizes).

over different time intervals concurrently. This capability to correlate over multiple discrete periods of time is especially useful in determining if suspect correlations are due to data issues or are in fact real disturbances. In this implementation, large window sizes correspond to 1200, 600, and 60 data points (20 sec., 10 sec., and 1 sec. respectively) and smaller, multi-cycle window sizes (54, 48, 30, 18, 12, and 6 data points) are used in order to assist with identifying the difference between data issues and power system events. A visual depiction of the window sizes used in a single case study can be seen in Figures 3.6 and 3.7.

3.2 Automated Wide-Area Protection

The goal of this Section is to explain the methodology behind the development of an automated wide-area protection strategy. The following subsections will address the modeling approach and grid topologies, discuss the specific experimentation considerations and implementation details, introduce the design of two key remedial action schemes, and finally describe the theoretical framework and implementation approach to the policy switching algorithm.

3.2.1 Time-Domain Dynamic Simulation & Power System Models

Power system simulation ranges from relatively simple, approximate approaches to more advanced time-domain, computationally complex, and high-fidelity approaches. There are advantages and disadvantages to each, but on the whole, power system modeling is an accepted method of analyzing system operation, long-term planning, and contingency studies, as well as validating new algorithms and approaches to controlling the grid. This Section discusses the use of time-domain dynamic simulation in order to test the policy switching algorithm (introduced in Section 3.2.3) on various grid models.

This research used three main grid models for various purposes. First, the IEEE 9-bus benchmark case was used for preliminary studies of simulator capability, $N-1$ security, and dynamics. Second, the IEEE 39-bus benchmark model was used for building, studying, and experimenting on the policy switching algorithm. Finally, the Polish grid model was used to further validate the established algorithm and assess its ability to scale to real grid topologies. One of the key takeaways of this research was defining and understanding the various power system models and their capability thresholds, primary control devices, and dynamic parameters. An exhaustive enumeration of the numerical assumptions, and dynamic parameters can be found in Appendix A.

3.2.1.1 The 9-Bus Model

The 9-bus model (seen in Fig. 3.8) was primarily used to determine the interfacing capability of various time-domain simulators. The initial attempts at developing the policy switching algorithm were implemented in PowerWorld. Unfortunately, although PowerWorld does have a transient simulation toolbox, the interfacing mechanisms for the simulator were not suitable to develop many of the modules necessary for the full design of this research. Through initial experimentation in PowerWorld, the author achieved a preliminary understanding of the software capabilities needed to construct N-1 secure and dynamic power system topologies. Therefore, the research is implemented in Siemens PSS/e which provides the necessary level of functionality needed to perform these transient studies while interfacing between the simulator and the algorithm.

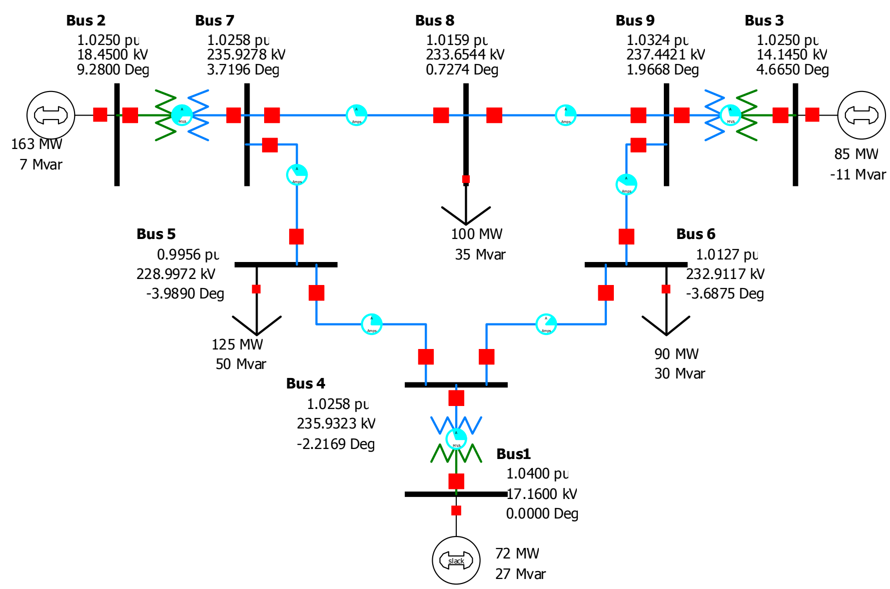

FIGURE 3.8: Visual representation of the IEEE 9-bus benchmark case.

3.2.1.2 The 39-Bus Model

The 39-bus grid model (seen in Fig. 3.9 [3]) is the primary test case used for analysis of the policy switching algorithm. Due to the decision to use Siemens PSS/e as the simulation tool, the functionality of the policy-switching algorithm was built in Python. This design choice provides suitable API interfacing capability, and also extends upon the software design of the PMU data analysis research (from Section 3.1) – also built in Python. The model of the 39-bus case allows one to explain and study the algorithm on a topology small enough for in-depth analysis of each bus. Following a single test case study, a larger randomized set of experiments is performed on the 39-bus case to better understand the performance of the algorithm.

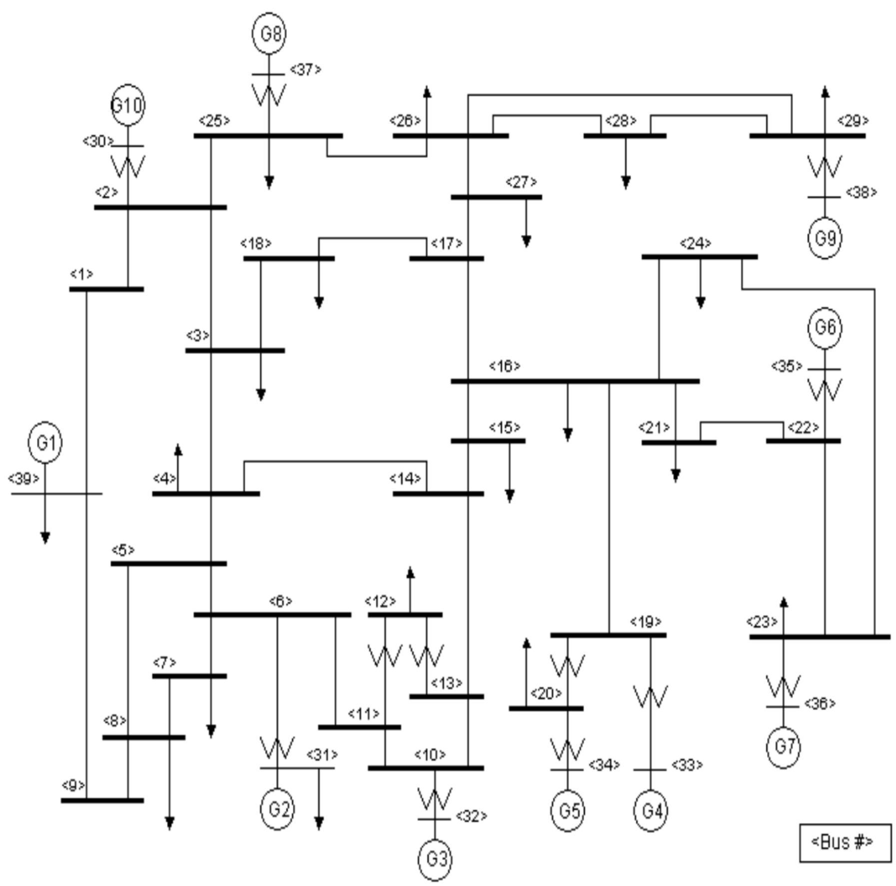

FIGURE 3.9: Visual representation of the IEEE 39-bus benchmark case [3].

3.2.1.3 The 2383-Bus Polish Grid Model

The polish grid model, developed from a model built in Matpower [61], consists of 2383 buses (Fig. 3.10), and is used to study the scalability and performance of policy-switching on a life-sized grid topology. This research experiments with a single case study N-2 contingency that is known to cause voltage collapse in the Polish network [62]. The results the experimentation on this model can be found in Section 4.2.

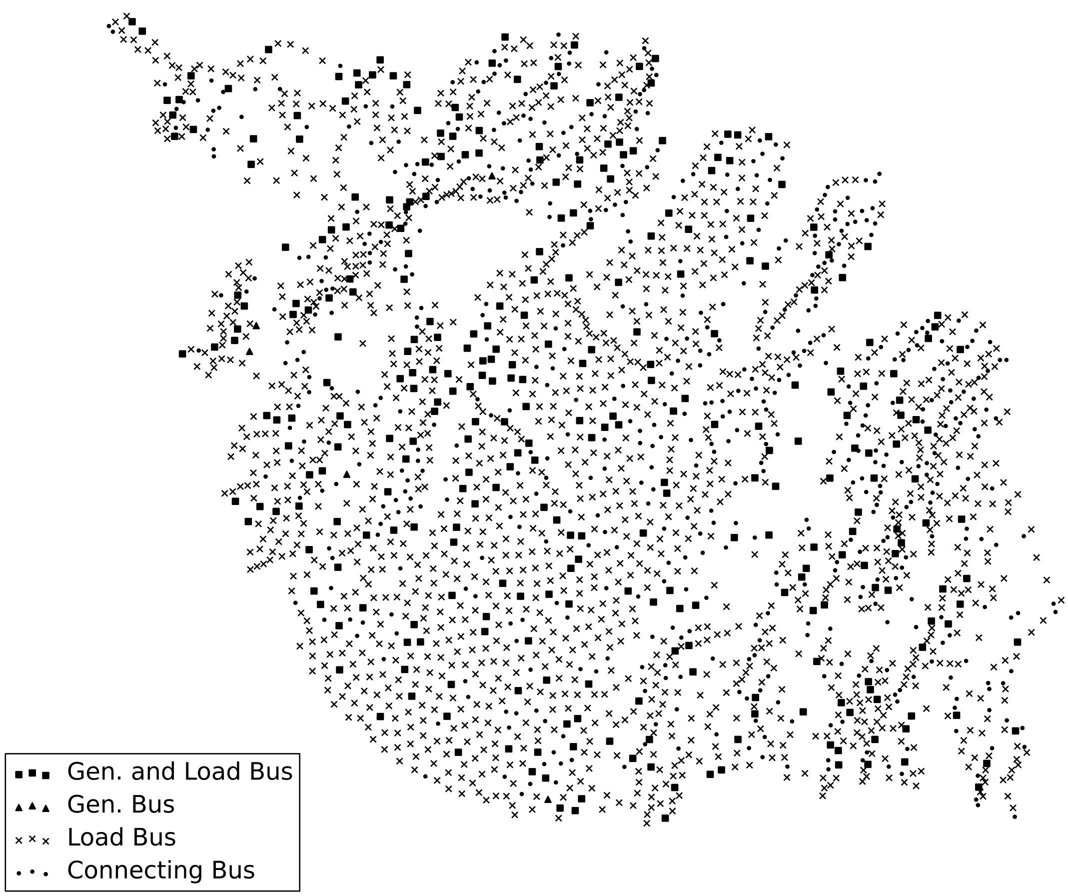

FIGURE 3.10: Visual representation of the Polish grid topology.

3.2.2 Design of Remedial Action Schemes for IEEE 39-Bus Case and 2383-Bus Polish Case

One of the novel aspects of the policy-switching methodology is that any RAS, and all of its possible permutations, can be implemented in a policy. This allows for testing of various RASs, and RAS combinations, over various emergency situations. In some instances, one RAS might perform better than another, and by allowing arbitrary switching between these different action-sets, it is possible to guarantee that an approximate optimal policy will be reached based on the value function it obtains over the duration of a single simulation. In the experimentation with this policy-switching methodology, two relatively simple RASs were used. This is in an effort to keep the focus on the algorithm and not the RAS itself.

3.2.2.1 Load Shedding (LS)

In both the Case-39 model and the Polish model, a simple homogenous load shedding technique, commonly used in utility protective methods today, is designed where each load in the system is decreased by a fixed ratio R [28]. This RAS is specifically chosen because of its ease of implementation, centralized approach to decreasing active and reactive power at each controllable load in the network, as well as its aptness to be performed online. More formally, load consumption is altered as follows:

$$L_{\text{final}} = \sum_{k=i}^{j} L_k \cdot (1 - R) \tag{3.10}$$

Where L_{final} is defined as the MVA power demand after load shedding, and L_k is each operational load at bus k, where k iterates over in-service load buses from the ith load bus to the jth load bus, and R is the fraction of load to shed. In this research, R is set to 0.1 so that each load sheds 10% of its nominal consumption each time the RAS is triggered.

3.2.2.2 Islanding (I)

The islanding RAS used in this research is an offline approach that seeks to split the individual models into separate generation and load-balanced microgrids according to pre-fault conditions.

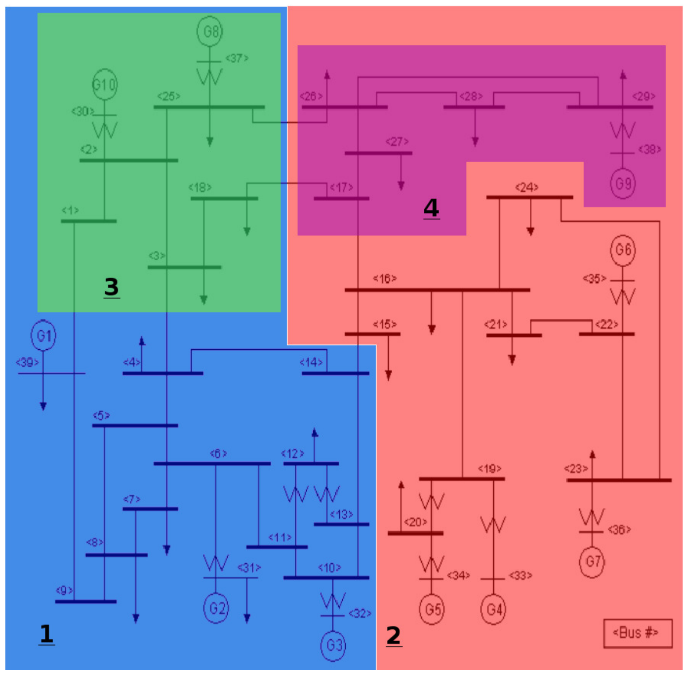

FIGURE 3.11: The islanding (I) rules for the policy switching experiments on the 39-Bus topology.

For the purpose of the 39-bus model experiments, there are two levels of islanding (I) capability that have been determined offline. Fig. 3.11 depicts an overlay of the islanding scheme with the 39-bus topology. The general concept of this method is to split the case, electrically, in half. This illustrative rule in Fig. 3.11 can be generalized to a proper measure of electrical distance that yields relatively stable islands in a slow-coherency sense, as proposed in [41]. Due to the small size of Case 39 it was determined that more than two iterations of this policy created islands that were not autonomous and therefore ineffective. For the first iteration, the case is partitioned into *Island 1* and *Island 2* (labeled and shadowed in blue and red in Fig. 3.11). The second level of islanding allows another split in half. Specifically, two sub-islands contained within *Island 1* and *Island 2* are created. As seen in Fig. 3.11, the two new sub-partitions are labeled *Island 3* and *Island 4* (shadowed in green and purple).

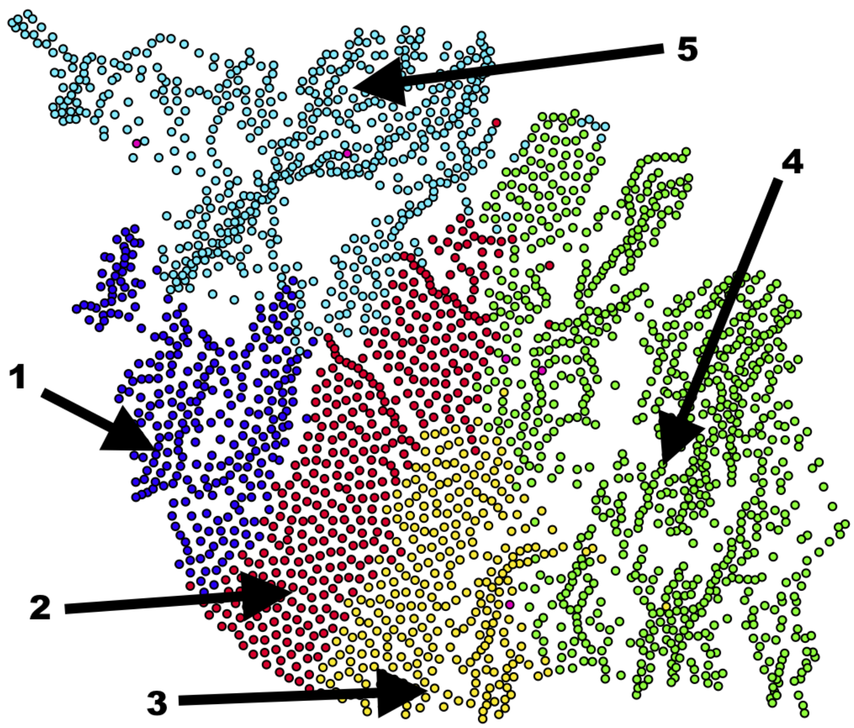

FIGURE 3.12: Islanding (I) strategy for the Polish grid topology.

In the Poland model, the islanding scheme is slightly more complex. It is still an offline-islanding method based primarily off of load and generation balance in microgrids, however each isolated sector of the Poland grid can be islanded independently of ordering. Figure 3.12 depicts the different sectors (microgrids) that can be disconnected and operated independently. The buses that fall into each of the five islands are colored similarly, and also depicted in the numbering scheme (1-5). When an islanding action is taken, the option for which of the 5 sectors to isolate is specified, and any or all can be islanded simultaneously.

3.2.3 Policy Switching

In many control applications, it is possible to obtain or create a set of diverse policies for which it is expected that at least one of the policies will perform well in any situation that may arise. For example, in the context of electrical networks, any existing RAS (and all of their parameterizations) is a possible policy. The main challenge in exploiting such a policy set, in practice, is that it is difficult to define rules for determining which policy is the best for a given state of the system. Policy switching [47, 63] is a control technique designed precisely for this situation. In particular, rather than attempt to compute an optimal policy, policy switching instead computes a policy that is at least as good in any state as any of the policies in a provided policy set.

3.2.3.1 Policy Switching Theoretical Framework

Policy switching assumes the availability of both a policy set $\Pi = \{\pi_1, \pi_2, \ldots, \pi_n\}$ and an MDP simulator. The simulator allows for starting in any state s and simulating any policy π in the MDP, resulting in a state and reward sequence. Note that for stochastic MDPs, the simulator may produce different results each run. Using such a simulator it is possible to compute an estimate $\hat{V}^{\pi}(s)$ of π's value function $V^{\pi}(s)$ from any state s. In particular, this can be done by conducting some number of Monte-Carlo simulations of π starting in s for a fixed time horizon and averaging the total discounted rewards across the simulations. This estimate converges rapidly to the true value as the number of simulations and time horizon grows[3] [64]. The availability of a reasonably accurate MDP simulator is realistic in many domains, including power systems. There are continuously

[3]Convergence is exponentially fast with respect to increasing the time horizon and the number of simulations.

improved research grade tools, as well as mature industrial grade simulators that answer a variety of problems for power networks.

Given the ability to estimate values using the simulator, policy switching uses a very intuitive approach to selecting actions. In particular, when arriving at state s in the actual system, policy switching computes the value estimate of each policy and then selects the action chosen by the highest valued policy. After selecting the action, the system transitions to a new state and the policy switching process repeats. Note that since all policies are considered at each encountered state, it is possible to switch between different policies over time. We propose a correspondence between these policies and the actions dictated by a RAS scheme for a given period of time. Formally, the policy switching policy over policy set Π, denoted by Π_{PS}, is defined as follows:

$$\Pi_{\text{PS}}(s) = \pi_{i^*}(s), \quad i^* = \arg\max_i \hat{V}^{\pi_i}(s) \tag{3.11}$$

where here i^* is the index of the policy that accumulates the maximum reward in state s using the simulator to estimate policy values. The computation time to obtain the policy Π_{PS} in state s scales linearly with the number of policies being considered. The run time is typically dominated by the simulations required for value estimates. Importantly, the algorithm can be easily parallelized since all simulations can be run on independent processors. This allows for an approximate linear reduction in runtime in terms of the number of available processors. This is important if one wants to consider large policy sets while also meeting real-time constraints on action selection.

It is not entirely obvious that it is safe in general to allow such free switching between any policy in a large set. However, this simple algorithm is able to provide the very strong guarantee that the value of the switching policy Π_{PS} in any state is at least as good as that of the best policy in Π. In particular, assuming that there is no approximation error in the value estimates $\hat{V}^{\pi_i}$ we get the following:

Theorem 3.2.3.1 (Adapted from [63]) *For any MDP, any policy set* Π*, and any state* s *we have that* $V^{\Pi ps}(s) \geq \max_i V^{\pi_i}(s)$.

Thus it is possible to leverage the potential benefits of switching without a system penalty. The above guarantee assumes that the value estimates were perfect, which will not be the case in reality due to both inaccuracies in the simulator and Monte-Carlo sampling. However, the result has been extended [47] to the case of approximate value estimates, where each value estimate $\hat{V}^{\pi}$ is guaranteed to be within ϵ of the true value. In that case, the above theorem is modified so that the value of the switching policy is no more than 2ϵ worse in value than the best policy in the set.

3.2.3.2 Policy Switching Implementation Approach

In order to implement the above theoretical policy switching framework (a visualization of this framework can be found in Fig. 3.13), the operation of the power system and its control strategies were abstracted into the context of MDPs, policies, and value functions in a suite of software designed in Python. The primary purpose of this section is to describe a few of the critical design choices and functionalities built into the Python code.

Recalling from section 2.4.1, an MDP is represented by a tuple – (S, A, P, R). In this power system modeling experimentation, the individual states (s) within the state-space (S), as well as the entire set of state transitions (P), are handled by PSS/e. This makes PSS/e a *hard simulator*. Since each state is a snapshot of the grid topology at a given time instant (all power flows, dynamic variables, device outages, etc.) the state-space is quite large. Therefore, the state representation in the Python code structure simply stores string characteristics that are pointers to binary files on disk. These state files allow reloading and revisiting previously encountered states in PSS/e – a functionality necessary for Monte-Carlo-based policy exploration.

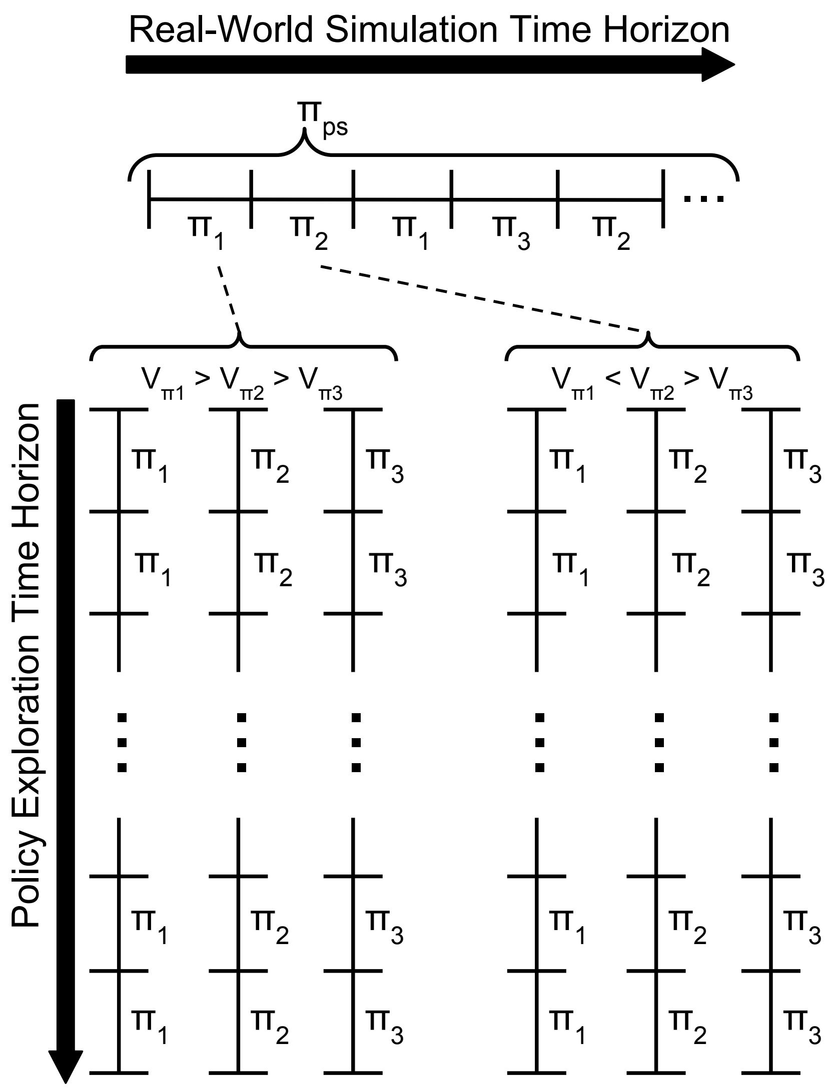

FIGURE 3.13: A visual representation of policy switching in the time domain.

In defining the allowable policies to be used in the policy-switching experimentation, the entire action-space (A) was used. Recalling from Section 2.4.2 a policy (π) is a mapping from states (s) to actions (a). In order to maximize the policy exploration over the course of the simulation, the policies are defined as the set of allowable permutations of the entire action-space (A). These *open loop policies* can therefore be considered non-stationary as they do depend on the time that the action is taken in the course of state transitions. Specifically, these open loop policies consist of the actions: "Do Nothing" (DN), "Load Shed 10%" (LS), and the various allowable islanding schemes (I). An important point here is that the level of RAS complexity, or number of allowable actions within a policy does not affect the theoretical basis of policy switching itself. This research simplifies the action-space and complexity of policies in order to make the point that this algorithm can be used to automatically find the best RAS, or combination of various RASs, to prevent voltage collapse during a severe contingency.

Finally, in the implementation of the policy-switching code, each policy's corresponding value functions (equation 2.9) needed to be evaluated since the value function determines the choice of the most optimal policy (π^*) at that decision time step. In evaluation of equation 2.9, β is chosen to be 0.98 so that values near the end of the simulation time horizon have a more significant weighting on the policy chosen at early decision time steps. Next, the method for allocating reward (r) to various states (s) was designed. Equation 3.12 depicts the reward function used.

$$r(s_t) = \begin{cases} \frac{L_t}{2 \cdot L_{total}} + \frac{A_t}{2} - \frac{B_{t-1}}{20} & : s = \text{terminal state} \\ -(\frac{B_{t-1}}{20} + \frac{C_t}{10}) & : s = \text{non-terminal state} \end{cases} \tag{3.12}$$

where t is the current decision time step, and $t-1$ is the previous decision time step. L_t is therefore the amount of operational load at the current time. The constant L_{total} represents the total load demand in the case. A is a boolean/binary variable that takes on the value 1 or 0 depending on whether the system was returned to a stable and acceptable operating point as a result of the policy.[4] B_{t-1} is a boolean/binary variable that takes on the value 1 or 0 depending on whether a RAS, such as Load shedding (LS) or Islanding (I), was used at the previous decision time step. C_t is a boolean/binary variable that

[4]In this context stable and acceptable is defined as all in-service bus voltages (V) satisfy the constraint: $0.9pu \leq V \leq 1.12pu$.

represents whether or not a single bus voltage violated the out-of-bounds constraints during a non-terminal state.

In short, $R(s_t)$ is a reward for an individual policy in state s at time t. It is defined as the weighted and normalized sum of the amount of operational load, and whether or not the power system was returned to a nominal operating point at the end of the simulation time horizon. In non-terminal states, the reward is either 0 or the policy is penalized if the system is unstable or an action other than "Do Nothing" (DN) is used in the previous decision time step.

3.2.4 Experimental Setup

In developing simulation-ready models, there were a few experimental considerations made that are worth noting. One of the main modifications to both the 39-bus model and the 2383-bus Poland model was made to their baseline security constraints. More specifically, both models were designed to be $N-1$ secure over the set of transmission lines in the case. This $N-1$ security assumption is important for the experimentation because the study involves analyzing the automated protection framework's ability to provide controls and stability during $N-2$ contingencies. The main U.S. utility regulation entities, NERC and FERC, currently require $N-1$ security, and this research is an effort to improve upon the status quo of current grid protection requirements by working toward a framework that may guarantee $N-k$ security.

In order to provide $N-1$ security, both models were modified by slightly altering the load and generation values, and by extending the rating limits for a few heavily loaded transmission lines. Each of the cases were then tested for transient stability and out-of-bounds (OOB) violations for every possible single line outage.

In building the experimental setup, the nature of the simulator (PSS/e 33) was carefully considered. Like many time-domain solvers, the analog (or continuous) nature of the real-world is approximated via discrete time steps. Figure 3.14 depicts the various

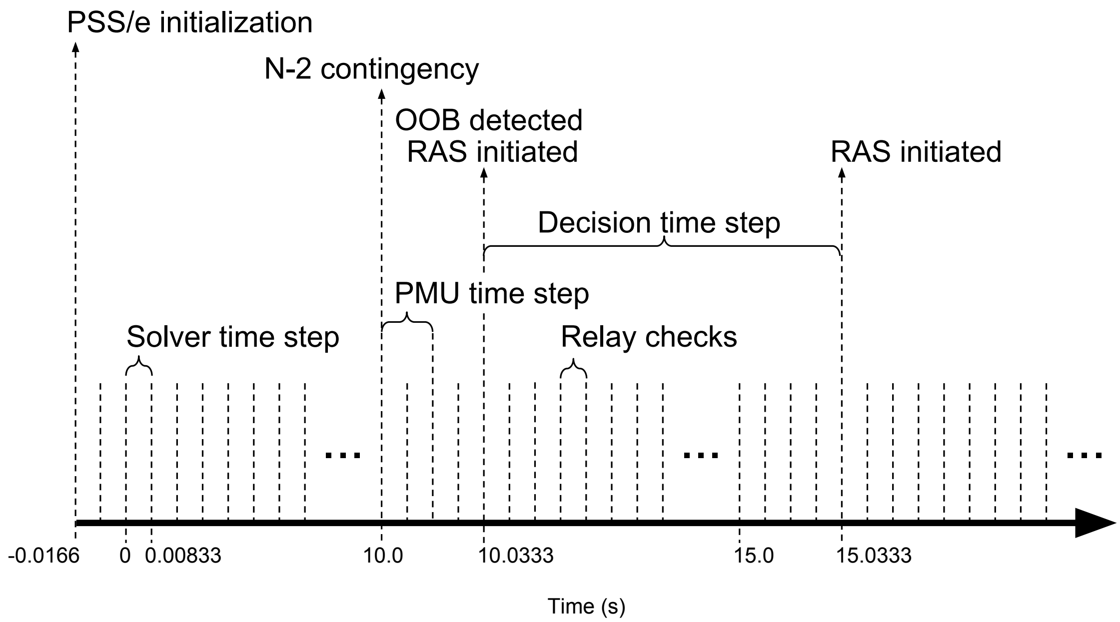

FIGURE 3.14: Example experimental setup depicting various time step sizes.

time steps for an arbitrary example run of the proposed algorithm in PSS/e. From the figure, it is apparent that the smallest step size, namely $\frac{1}{120}$ sec. is the solver step size. The PSS/e operation manual suggests that a step size of at least half the operational frequency be used [52]. Next, the author defines additional step sizes for various operations on the models. Immediately after the initial $N-2$ contingency, a step size of $\frac{1}{60}$ sec. is defined in order to mimic an incoming PMU data stream. Out-of-bounds (OOB) violations are therefore only identified at this time scale. An additional *decision time step* is defined for the policy switching algorithm. This is a five second time step that is based on the settling time of the primary governor and exciter responses. In the real world this would mimic an operator's various decision points in initiating RASs to recover from an emergency situation. It does not make sense to place RASs too close together because dynamic responses to these actions might result in voltage collapse or additional failures that are artificially caused by the operator.

4 RESULTS

This chapter will describe the details of the experimentation performed and results gathered for both the automated PMU data analysis functionality and the automated protection methodology. Section 4.1 will cover the specific findings associated with the correlation studies of the PMU data. Following that, Section 4.2 will cover the results obtained during experimentation on various grid models using the theoretical framework of policy switching to protect against, and recover from, emergency contingency situations.

4.1 Automated PMU Data Analysis Results

This section focuses on highlighting some of the preliminary qualitative information obtained by processing and analyzing the PMU data streams via the correlation methodology. The research is intended to be a stepping stone in automated identification of events such as the ones listed in Table 4.1. The results will be organized as follows, section 4.1.1 begins with a short introduction to the visualization technique developed for analyzing the different data and power system events. Sections 4.1.2 and 4.1.3 will then portray the visualization of different data and power system events. Finally, Section 4.1.4 will depict some of the preliminary work done in using the correlation methodology to identify PMU cyber-data attacks.

4.1.1 Visualization Structure

The purpose of this subsection is to introduce the layout of the visualization structure. A sample is seen in Figure 4.1. A few noteworthy points are as follows: each coordinate (square) represents the correlation coefficient of the two PMUs that make up its coordinates (numbered PMUs 1-20). The color of the square represents how close

TABLE 4.1: Data and Power System Event Signatures

Data Event	**Expected Identifier/Description**
Data Drop	V† and/or ϕ^* data $= 0$
PMU Misread	Repeated values over multiple time steps
Loss of GPS Synchronization	ϕ drift, PMU units not synced
Power System Event	**Expected Identifier/Description**
Power Flow Contingency	Change in $\frac{d\phi}{dt}$
Generator/Load Trip	Change in V and/or $\frac{d\phi}{dt}$
Transmission Line Trip	Change in V and/or slight change in ϕ
Power Transformer Tap Change	Change in V
Miscalibration of Transformer	Pending further investigation
Capacitor/Reactor Switching	Change in V and ϕ
Inter & Intra Zone Oscillations	Slow-coherent change in V or ϕ

† V = Positive sequence bus voltage magnitude

* ϕ = Positive sequence bus phase angle

the correlation is to 1 or -1, and the sign at the coordinate represents either positively correlated or inversely correlated PMU pairs. Typically a magnitude of correlation above $0.4 - 0.5$ is considered correlated. Thus any squares depicting blue shades would be considered de-correlated. It is important to keep in mind that this visualization is temporal, and represents different time window lengths as discussed in Section 3.1.4. The metric of electrical distance is also incorporated here, because each coordinate of the upper triangular matrix is related, electrically, back to PMU 1. In effect, an increase in PMU number

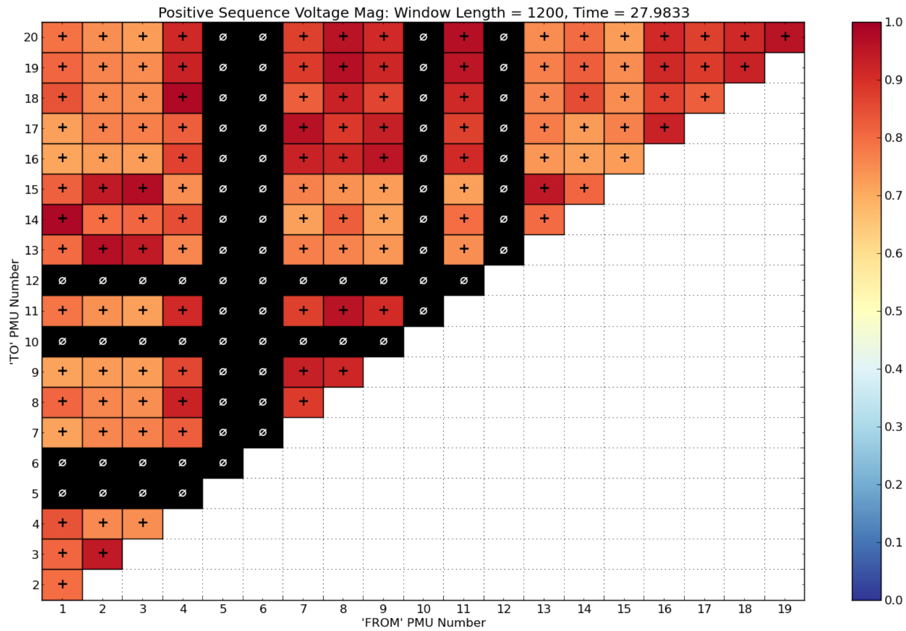

FIGURE 4.1: Example PMU correlation visualization over 1200 data point window (20 seconds).

also corresponds to an increase in electrical distance from the reference node (PMU 1).

4.1.2 PMU Data Inconsistencies

The primary goal of this research thrust is to develop a methodology for automatically discerning operational information from the massive amounts of sensor data being produced by multiple PMUs throughout the system. The first step in achieving this is the ability to differentiate between common PMU data errors and actual power system contingencies. Two of the most common PMU errors, highlighted in the first two rows of Table 4.1, are data drops and communication or sensor errors.

The first issue, data drop, is typically characterized by the PMU shutting off or restarting – resulting in zeroed data over large window sizes as seen in image 4.2. This is particular data issue is represented by the blacked out "null" rows and columns indicated in the example visualization (Fig. 4.1). Using this correlation methodology it is possible

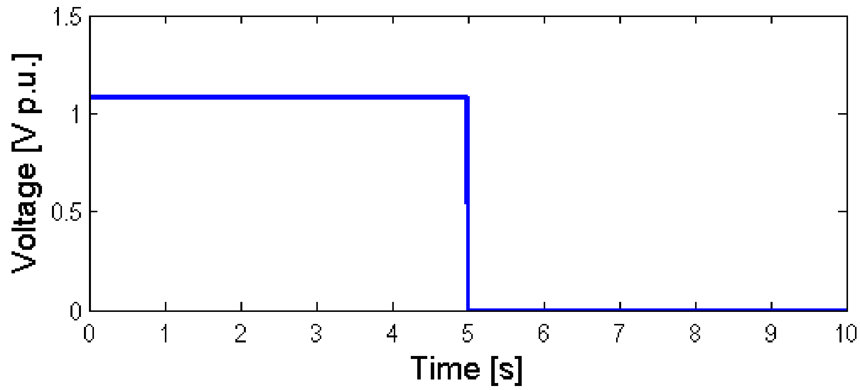

FIGURE 4.2: Example of a raw voltage signal data drop.

to flag consecutive sets of zero data. From the visualization, it is detected that PMUs 5, 6, 10, and 12 were not logging data during this particular time frame in the BPA dataset.

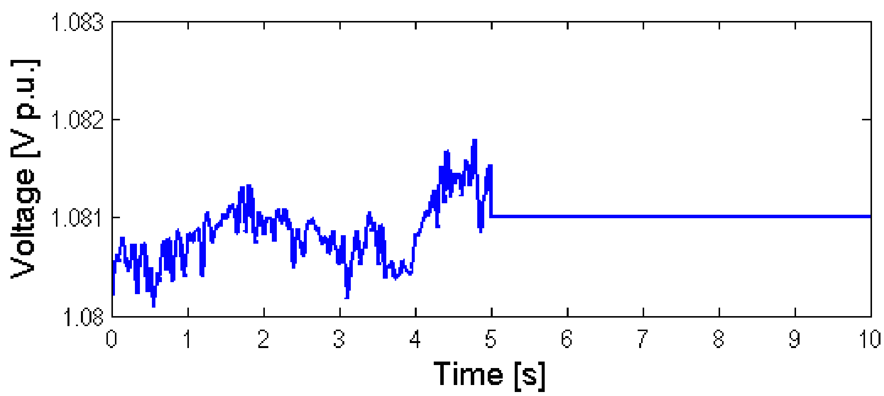

FIGURE 4.3: Example of a PMU misread on the raw voltage signal.

The second data issue, PMU misread or communication error, is depicted in Figure 4.3. Though it is not immediately obvious (since our data issues are both depicted with the "null" symbol) an explanation follows.

Figure 4.4 depicts a short time series of plotted correlation matrices. Each correlation value is determined over a sliding window of length 2 (or $2 \cdot \frac{1}{60}$ sec = 0.0333 sec). This short duration is why the correlation coefficients are exactly 1.0. The goal of this figure, however, is to show how the algorithm can isolate and recognize possible communication

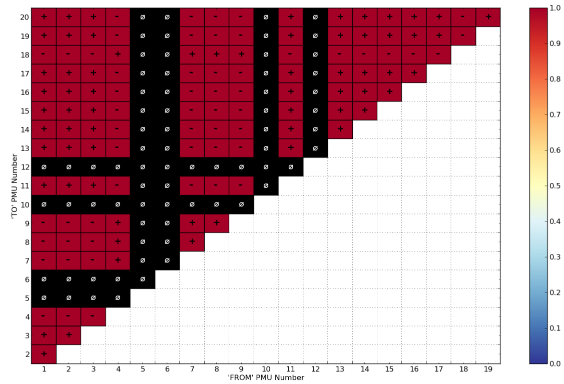

(a)

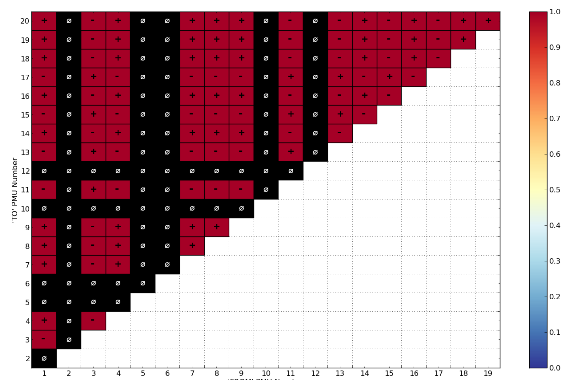

(b)

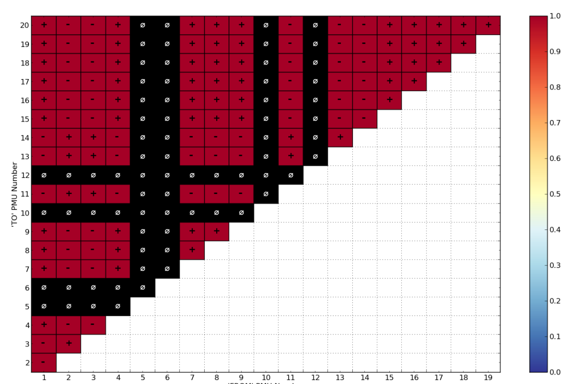

(c)

FIGURE 4.4: Time series of correlation matrices depicting PMU misread detection at a window size of $\frac{2}{60}$ sec.

or sensor errors. Panels (a), (b), and (c) from Figure 4.4 occur over a time period of $\frac{3}{60}$ of a second, and in that short time, PMU 2 produces data that is identically the same as the previous time step (seen by column 2 and row 2 being blacked-out in panel (b)). Instead of flagging this anomaly as a power system contingency or data drop, one can recognize the short time duration, and the immediate return to normal operation (from panel (b) to (c)) as a communication error.

4.1.3 Clean Dataset versus Lightning Event

This section describes the results of the correlation algorithm and its ability to detect power system events. The PMU data obtained from BPA contained various known power system contingencies. The majority of these events were lightning strikes on transmission lines either causing permanent outages, or causing fault symptoms that grid protection devices (such as relays and reclosers) were able to recover from.

To test the automated PMU data analysis framework, the author compares clean power system data and lightning event data. The results can be seen in Figures 4.5 and 4.6. By observing the images, it becomes apparent that there are patterns of correlation amongst the voltage magnitude and phase data that can serve to automatically identify power system contingencies.

4.1.4 PMU Cyber-Security Considerations

The correlation approach to automatically analyzing PMU data was also considered as a possible solution for data cyber attacks. This section reviews the results of using the correlation framework to automatically identify a data spoofing attack on a single PMU. In order to fabricate a PMU data spoof, a single PMU's data was mirrored and repeated over half of the observed time window. There are many other possible data spoofing methods, however in order to validate our identification method we use this mirroring method because it is not fabricated data, rather it is a replay of real PMU data that has

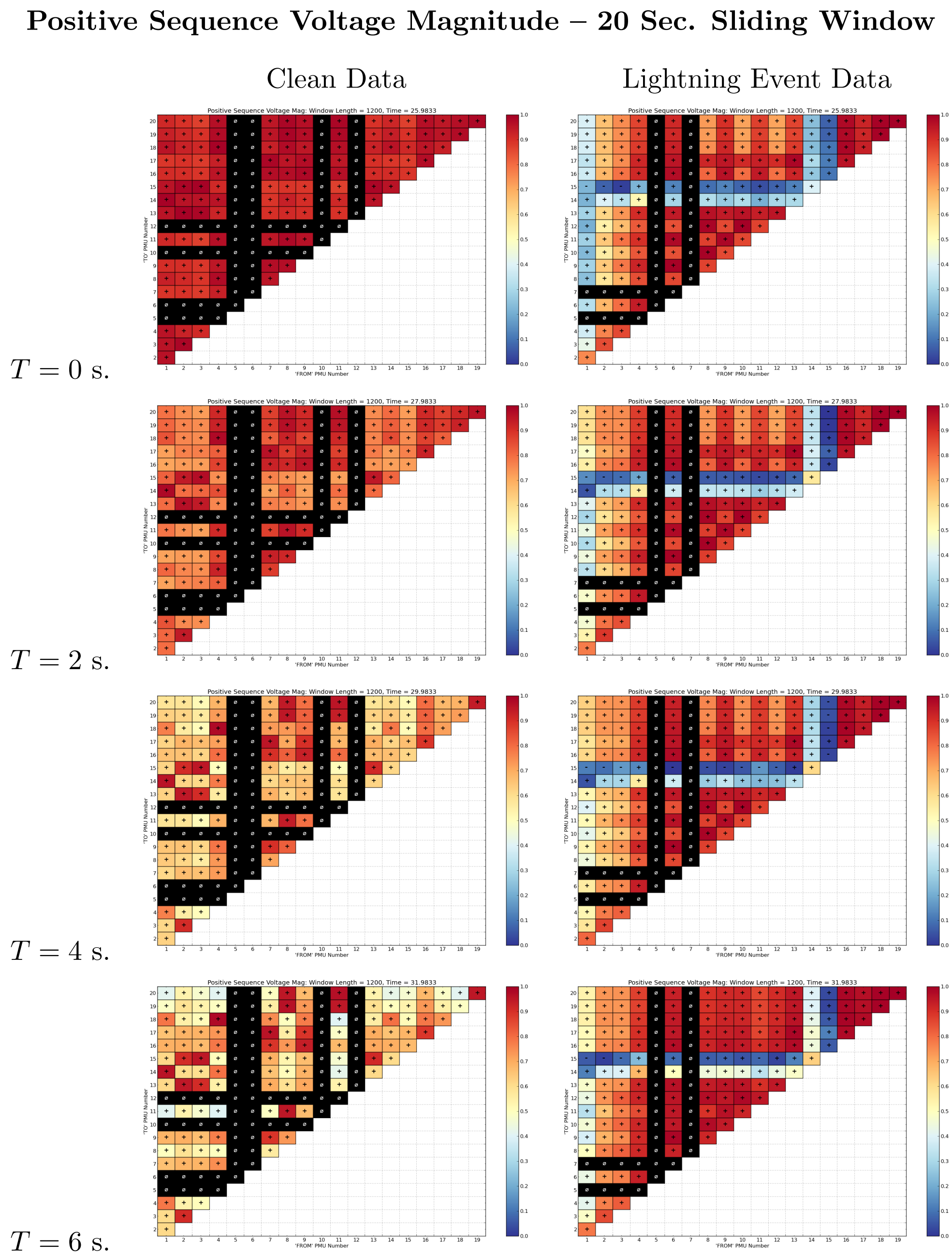

FIGURE 4.5: Clean data vs. lighting event visualization – voltage magnitude.

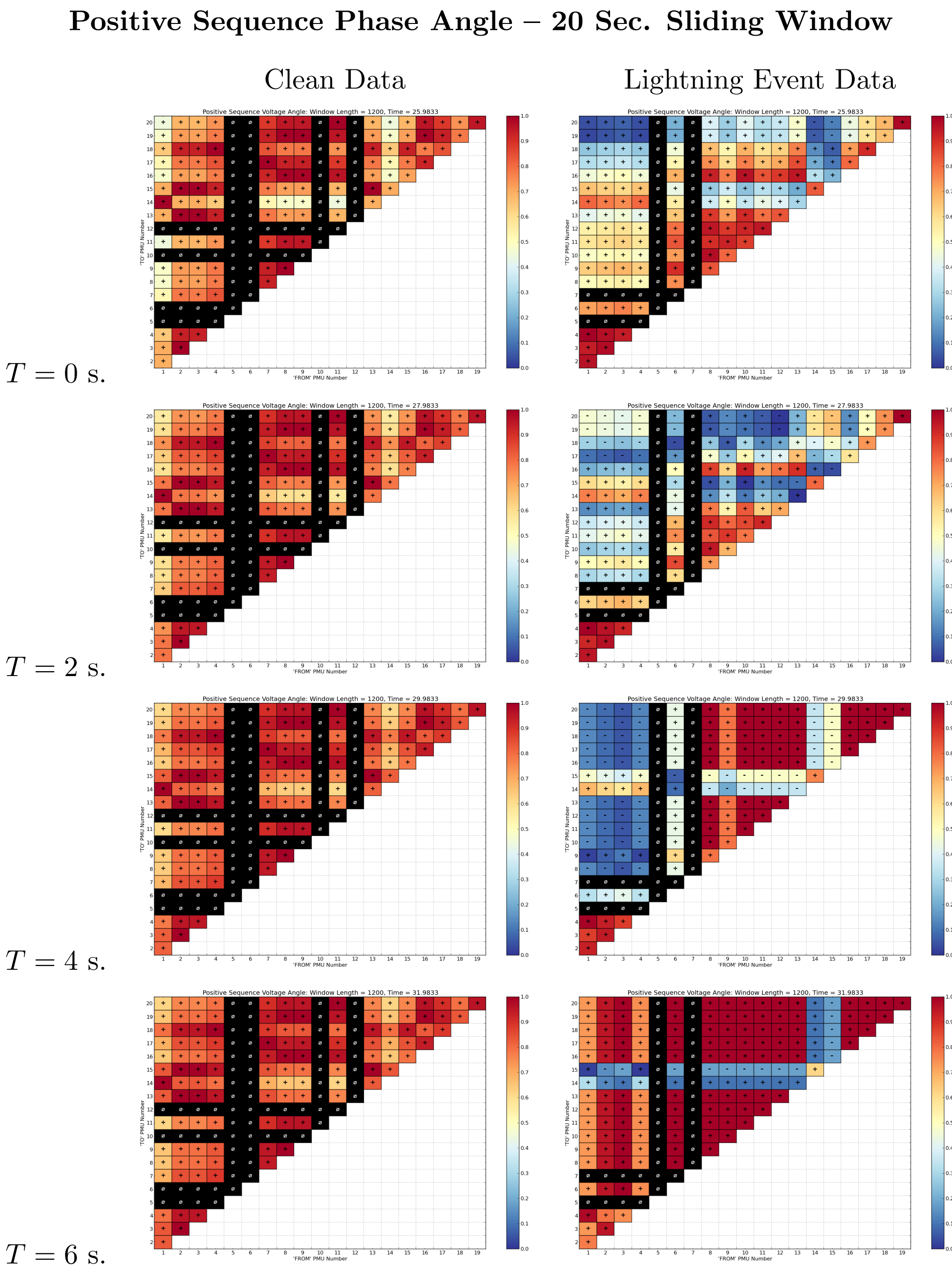

FIGURE 4.6: Clean data vs. lighting event visualization – phase angle.

already been seen. A plot of the correlation results of the frequency (f) data stream can be seen in Figure 4.7.

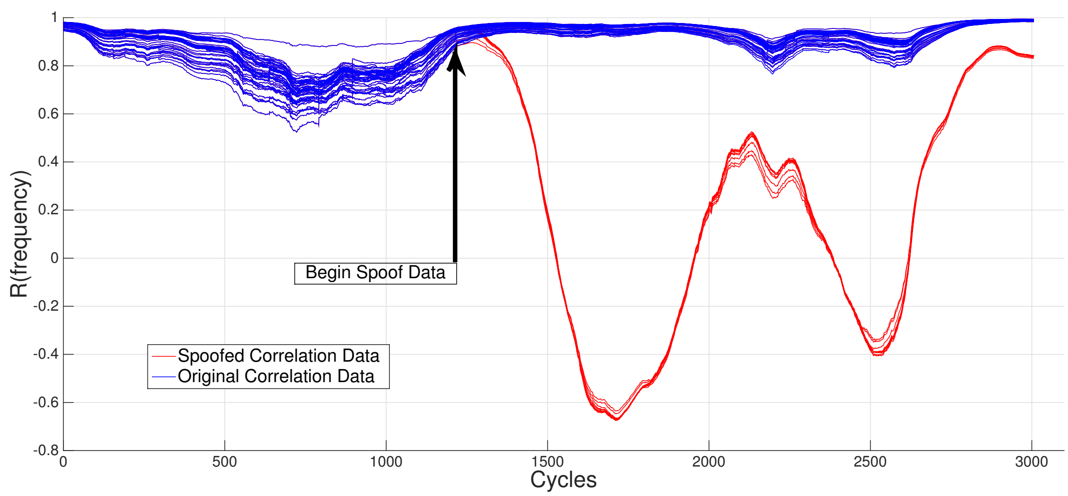

FIGURE 4.7: Frequency correlation data (calculated over a ten second window size) for ten electrically close PMUs.

From the figure, one can see the decorrelation of the PMUs that are paired with the spoofed PMU signal. This qualitative ability to determine when PMU data is being artificially generated, even from its own past data, is critical to identifying when that data is being spoofed.

This research investigates this same phenomena over each of the various PMU data signals (f, V_{+Mag}, $V_{+\phi}$, $V_{0\phi}$ and $V_{-\phi}$) as well as over multiple correlation window sizes. This is an effort to characterize any differences between the correlation algorithm's ability to detect spoofing on different signals. Instead of depicting the many graphs generated from this effort, the author constructed two indices to measure the deviation of the spoofed versus original data. The two indices are described below:

Maximum Correlation Deviation (MCD): A measure of the maximum difference between the non-spoofed ($nspf$) data and the spoofed (spf) data, formally calculated as an element-wise Euclidean distance:

$$MCD = max\left[\sqrt{(\text{nspf} - \text{spf})^2}\right] \tag{4.1}$$

Maximum Correlation Out-Of-Bounds time (MCOOB): A measure of the amount of time that the spoofed data remains outside of a ±10% bound on the non-spoofed data. Formally, this is calculated as a summation of the time where the following inequality is satisfied:

$$MCOOB = \Sigma_{cycles}\,(0.9 \times \text{nspf} > \text{spf} > 1.1 \times \text{nspf}) \tag{4.2}$$

Given the indices described in equations 4.1 and 4.2, each of the PMU data stream were analyzed and consolidated in Table 4.2.

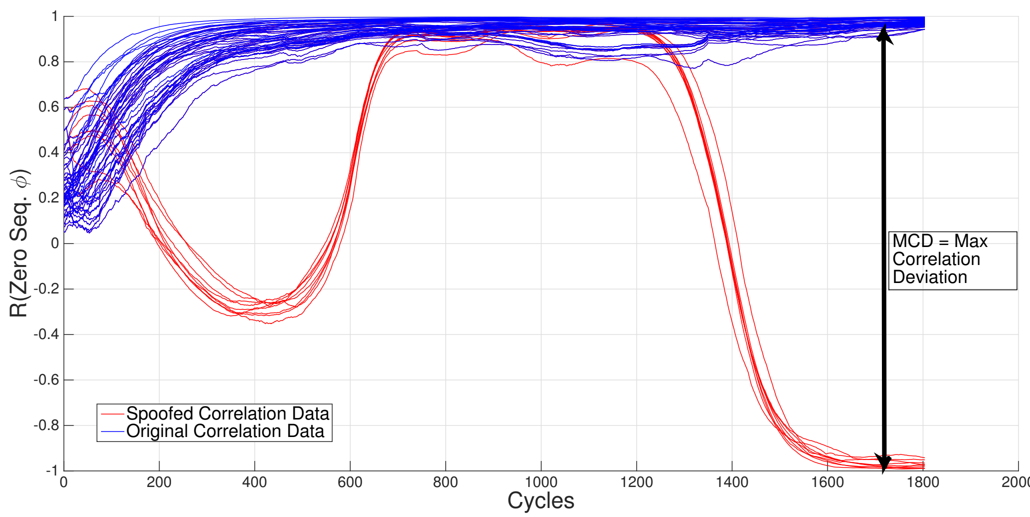

FIGURE 4.8: The MCD metric visualized on the zero sequence voltage phase angle PMU data stream.

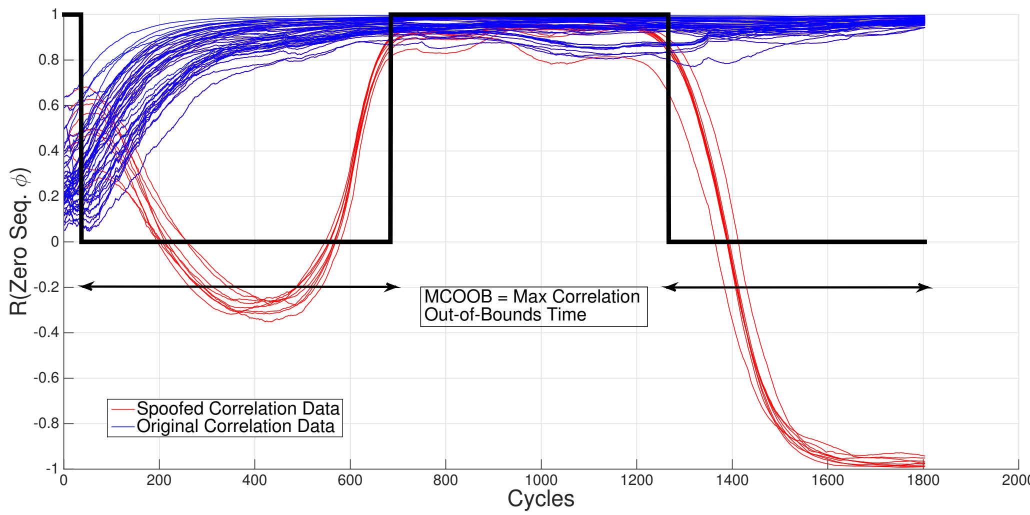

FIGURE 4.9: The $MCOOB$ metric visualized on the zero sequence voltage phase angle PMU data stream.

TABLE 4.2: This table depicts the two indices that represent the severity of decorrelation during spoofing. Each entry represents a graph of its corresponding window size and PMU parameter. The bolded entry represents the data presented in Fig. 4.8 and Fig. 4.9. Entries are in the format: $[MCD, MCOOB]$.

	f	V_+	ϕ_+	ϕ_0	ϕ_-
60 cycle	[1.34, 29.30]	[1.93, 28.48]	[2.00, 18.18]	[1.93, 28.73]	[1.96, 28.90]
120 cycle	[1.43, 28.38]	[1.93, 28.33]	[1.99, 18.40]	[1.96, 25.15]	[1.98, 26.40]
300 cycle	[1.65, 28.65]	[1.77, 29.23]	[1.99, 18.41]	[1.98, 23.18]	[1.99, 25.30]
600 cycle	[1.64, 27.70]	[1.33, 28.58]	[1.99, 19.70]	**[1.98, 22.56]**	[1.99, 24.76]

4.2 Automated Protection Framework Results

This section will cover the results obtained for the policy switching methodology. Three main results will be covered in the subsections below. First, Section 4.2.1 will analyze a single $N-2$ contingency on the 39-bus grid model. This contingency situation, and the operation of the policy switching algorithm will be covered in detail in this section. Next, Section 4.2.2 will provide the results to a study of 100 random N-2 contingencies on the 39-bus model. Finally, a single case study will again be presented, in Section 4.2.3, that depicts the operation of the policy-switching algorithm on a life-size grid topology – the Polish grid model.

4.2.1 39-Bus: Test Case Study

This case study on the 39-bus model analyzes the N-2 contingency that cuts the transmission lines between buses 2-25 and 19-20. Figure 4.10 depicts the location of these two exogenous events, as well as the subsequent line relay trips and islanding action taken when policy switching is invoked.

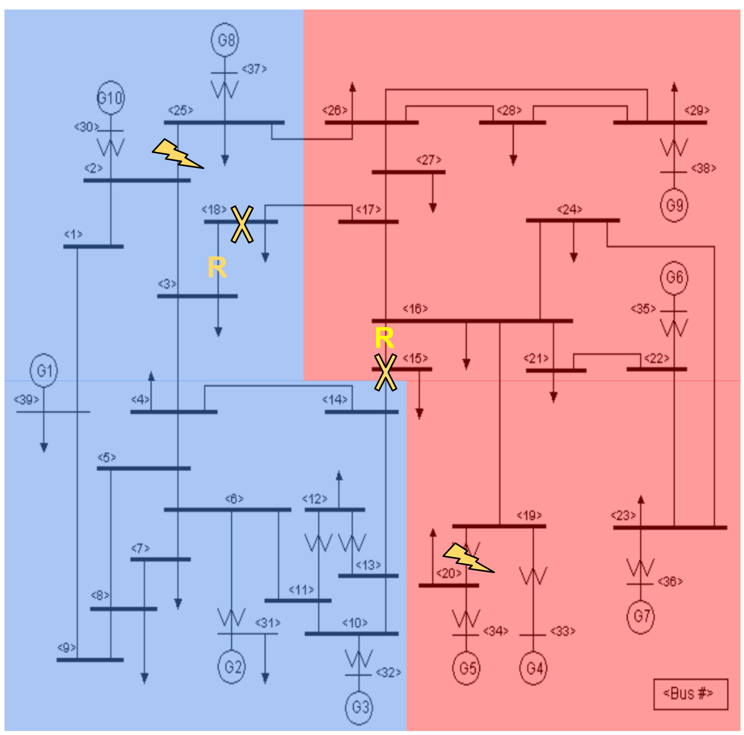

FIGURE 4.10: Layout of the case study N-2 contingency on the 39-bus model (with policy switching enabled).

TABLE 4.3: 39-Bus Case Study Results

General Policy Set (Π)	Most Successful Policy ($\pi^*(s)$)	$V^{\pi^*}(s)$	Result Note
No PS	-	-	Voltage Collapse
LS action only	{LS, LS, DN, DN}	0.5462	Stability maintained with 5185 MVA Load†
I action only	{I, I, DN, DN}	-1.079	Voltage Collapse
LS & I actions	{LS, I, DN, DN}	0.5552	Stability maintained with 5434 MVA Load†

†Pre-fault Load is 6453 MVA

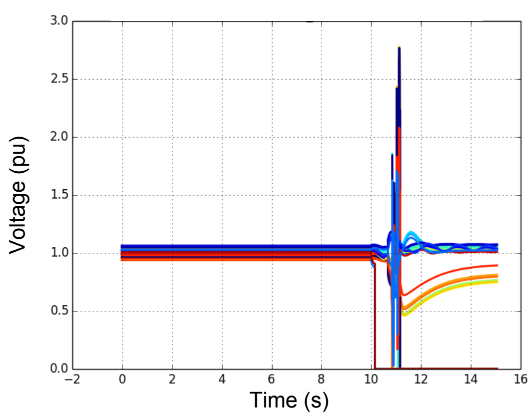

(a) Graph of bus voltages without operational control.

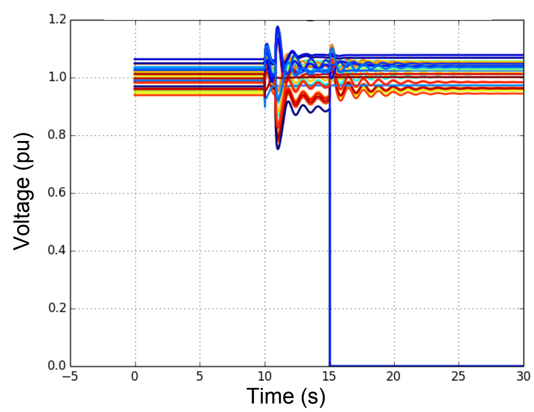

(b) Graph of bus voltages with policy switching activated.

FIGURE 4.11: Graph of voltage profiles over N-2 Case Study simulation time horizon.

From Table 4.3, it is apparent that the policy-switching policy (π_{ps}) is the most optimal policy to follow during the course of this particular emergency situation. By doing nothing, or by simply allowing permutations of the islanding RAS, the severity of the $N-2$ contingency case study causes voltage collapse. However, according to the value function of the combined LS and I policy, the policy-switching algorithm is able to determine that the optimal course of action to take is to first load shed, then island in half, and then do nothing for the remainder of the simulation.

A comparison of the voltage profiles for both the non-policy-switching simulation, and the implemented optimal policy can be found in figure 4.11, and an enumeration of each event during the π_{ps} simulation can be found in figure 4.12.

4.2.2 39-Bus: Set of $N-2$ Contingencies

In order to sufficiently test the policy switching algorithm and its ability to act as an automated wide-area protection methodology, a set of 100 random $N-2$ contingencies are invoked on the 39-bus model. Each of these 100 experiments are fully simulated *without* policy-switching implemented, and again simulated *with* policy-switching activated. Table 4.4 enumerates the entire set of $N-2$ contingencies by enumerating the various experiment result counts. Following that, Table 4.5 enumerates a few of the load metrics from the set of 100 simulations. Finally, Table 4.6 shows the timing statistics for the various contingency simulations run. Section 5.1 will cover the discussion and key takeaways of the results depicted in this section.

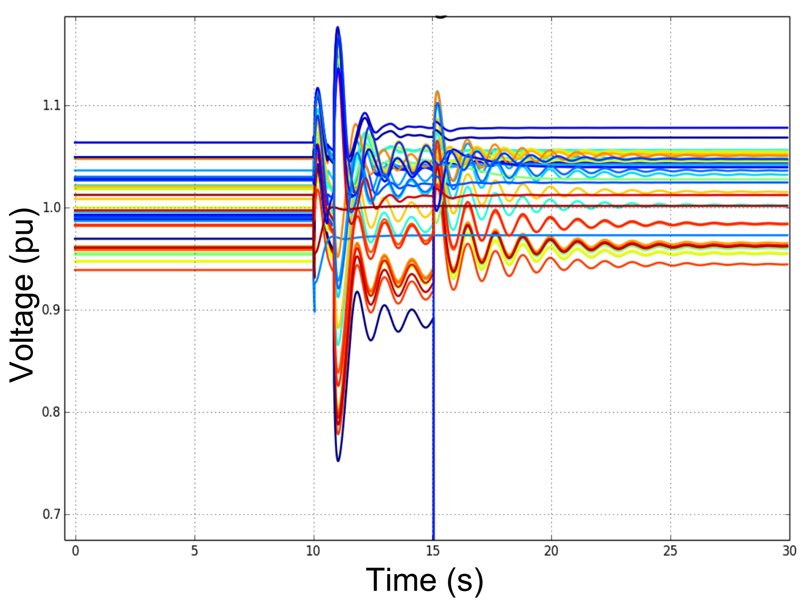

-0.0167 s. = PSS/e initialization

10 s. = N-2 contingency invoked

10.0499 s. = OOB detected, Policy switching started,
LS action taken

10.599 s. = Line relay trip (line 3-18)

10.866 s. = Line relay trip (line 15-16)

15.0499 s. = Island action taken (two isolated buses, 15 and
18 set to out-of-service)

20.0499 s. = Do nothing action taken

25.0499 s. = Do nothing action taken

30 s. = End simulation

FIGURE 4.12: Enumeration of the events that occur during the π_{ps} solution of the 39-Bus test case study.

4.2.3 Poland 2383-Bus: Test Case Study

In developing a test case study for the Polish grid model, it was important to first identify an $N-2$ contingency that was severe enough to affect the grid stability. In doing this, the author relied on information gathered from a dc stability study in [62]. Song et. al. implemented a dc simulation on the 2383-bus model in order to determine rankings

TABLE 4.4: 100 Random $N-2$ Contingencies – Experiment Count Comparison

No Policy Switching		Policy Switching	
Simulation Result	Count	Simulation Result	Count
No OOB Detected	16	No OOB Detected	16
Voltage Collapse	37	Voltage Collapse	6
Unstable Terminal State	5	Stable and Less Operational Load	1
Stable Terminal State	42	Stable and Equivalent Operational Load	36
-	-	Stable and More Operational Load	41

TABLE 4.5: 100 Random $N-2$ Contingencies – Loading Statistics

Average Load Lost due to $N-2$ Contingency†	
No Policy Switching	Policy Switching
2967.1 MVA	692.08 MVA
Average Load Improvement*	
4674.87 MVA	

†Excludes the 16 experiments that were not severe enough to cause OOB violations.

*Only considering the 41 experiments that improved amount of operational load.

of the most severe $N-2$ contingencies. Since the research presented here uses dynamic simulation, finding a suitable $N-2$ contingency to test the policy-switching algorithm was not an exact science, however, the results from the dc simulator were used to inform the author about which transmission lines in the case were critical flow paths during off-nominal situations.

TABLE 4.6: 100 Random $N-2$ Contingencies – Policy Timing

Policy Action Count and Timing[1,2]				
	Decision Time Step			
Action	1st	2nd	3rd	4th
LS	21	3	0	0
I	17	1	0	5

[1]There were 42 simulations that used a policy other than: {DN,DN,DN,DN}

[2]4 simulations used a mixed-action policy.

By using the findings from the dc simulation, the author chose to implement the $N-2$ contingency that opens the transmission lines between buses 138–167 and 1876–1875. Similar to the experimentation in the test case study on the 39-bus system, this research compares the success of the policy switching algorithm to those of "Do Nothing" actions, as well as policies that only have one action available. These results can be seen in Table 4.7.

TABLE 4.7: 2383-Bus Poland Case Study Results

General Policy Set (Π)	Most Successful Policy ($\pi^*(s)$)	$V^{\pi^*}(s)$	Result Note
No PS	-	-	Voltage Collapse
LS action only	{LS, DN, DN, DN}	-1.079	Voltage Collapse
I action only	{I_5, DN, DN, DN}	1.638	Stability maintained with 18546 MVA Load†
LS & I actions	{I_5, LS, DN, DN}	1.591	Stability maintained with 16705 MVA Load†

†Pre-fault Load is 18601 MVA

5 CONCLUSIONS AND FUTURE WORK

5.1 Conclusions

This research has introduced multiple contributions to the study of automated decision-making in the context of power systems protection. As presented in Figure 1.1, each of the sub-blocks implemented in this work are meant to contribute to the vision of a future grid operational framework that leverages modern sensor technology, data processing, communication protocols, pattern recognition, and automation of controls to protect the grid. Unfortunately, this level of automated protection and control is difficult to achieve without further advances in the ability to monitor the grid. For that reason, this research not only studies automated decision-making in protection, but also includes some preliminary work on developing automated wide-area monitoring and analysis tools.

The results, as presented in Section 4.1, show promising qualitative ability to distinguish between nominal operation, PMU sensing errors, and actual power system events. Figures 4.5 and 4.6 depict the concept quite well – that is the evident decoration of PMU pairs during a lightning event on the grid when compared directly to known clean data. It is also apparent that using the correlation methodology to identify spoofing events is possible, due to the separation of those PMU signals that are spoofed from those that are not. This is seen in Figure 4.7 as well as in the indices representing the magnitude of decorrelation in Table 4.2. These types of separation-of-data problems are well served by modern machine learning techniques. It can be concluded that this correlation method, when paired with a fast database architecture, as developed in [11], has real promise for being an advanced and automated tool to improve operator decision-making for wide-area monitoring in a variety of power system operating scenarios.

Section 4.2 presents results for the automated wide-area protection algorithm developed in this research. The test case study on the 39-bus model demonstrates how the algorithm is able to find the policy with the best value at each decision time step in the simulation time horizon. Figure 4.12 indicates the various actions that occur while following the policy switching policy (π_{ps}) in the real world. Comparing the output of the simulation that did not use policy switching, it is apparent that the algorithm was able to save the system from voltage collapse, and from Table 4.3 the amount of operational load was also saved by following π_{ps}.

Tables 4.4, 4.5, and 4.6 all depict the results gathered from the statistical study on the 39-bus model. This set of 100 random $N-2$ experiments resulted in multiple cases where the policy switching algorithm was able to optimally save the network from voltage collapse according to the policies that were available to it. One particularly interesting result can be seen in Table 4.6. Here, the actions taken at each of the five second decision time steps are enumerated over the 100 contingencies studied. The first column (1st decision time step) indicates that the policy switching algorithm found that load shedding was the first action to take in some scenarios (about 50% of the time), whereas in other cases islanding the grid in half was the best action to use (about 41% of the time). Table 4.5 supports the success of policy-switching in maximizing operational load; it shows that out of all the 100 simulations, there is a distinct difference in the average amount of operational load lost during an $N-2$ emergency situation – the average difference being about 2275 MVA or about $\frac{1}{3}$ of the topology's power demand.

Finally, in order to verify the findings of policy switching, this work analyzes the performance of this automated protection framework on a life-sized grid model. Section 4.2.3 discusses the results of simulating another test case study on the 2383-bus Polish grid model. From Table 4.7 it is evident that the most successful policy, according to its value function and the amount of operational load at the terminal state, is islanding section five of the polish model (see Figure 3.12 for the five different islanding sectors).

In conclusion, the author found that within any set of defined protection policies there is a unique combination of protection measures that optimally return the electric grid to an acceptable and stable state. Perhaps nonintuitively, this combination of protection measures is not necessarily a single one-size-fits-all RAS. Rather, for the nearly infinite number of contingencies, both exogenous and endogenous, there will be a specific order of protection measures that must be implemented to optimally save the power network from off-nominal modes that have the potential to develop into cascading outages. Policy-switching provides an algorithmic means to determine which RAS policy should be implemented and avoids presupposing the individual solution to any specific contingency. This is becoming increasingly important, especially as more complex constraints are introduced into grid operation such as variable renewable generation, large storage capability, increased grid congestion, aging infrastructure, and demand for high quality electric power.

5.2 Future Work

This Section will address a few of the author's ideas for furthering this work. For the wide-area monitoring and PMU research, there is still a significant amount of quantitative identification needed in order to make this a viable automated PMU analysis tool. Judging from ongoing collaborative work that the author is involved with, various machine learning techniques such as artificial neural networks and support vector machines are good options for classification of this high-cardinality data. Another significant aspect in furthering this work will be to assess the online capability of the algorithms used. Much of power systems operation occurs in real-time, and having significant delay in the identification mechanism could lead to downstream problems with dispatch and control of electric power.

The automated protection framework and use of the policy-switching algorithm for wide-area grid protection and decision-support can also benefit from additional studies. One key adaptation needed in validating the success of policy-switching in real-time grid environments will be to add stochasticity to the power systems models. The studies performed in this work are deterministic. Also, the policy-switching methodology could be improved by expanding the action-space of RASs, adding further metrics for the policies' ability to assess grid states, and improving the reward function by perhaps including load priority, economics of generation, and severity of instability. Finally, this algorithm is computationally slow due to the dynamic simulation coupled with Monte-Carlo-based evaluation. Simulation time, even on a dedicated server, is on the order of hours or days. For that reason, this framework would benefit greatly from parallelization of the policy rollout. Also, according to current research thrusts that the author is collaborating on, it may make sense to utilize a multi-fidelity simulator. Specifically, a dc simulation could be used for immediately ruling out failed Monte-Carlo search paths. This would dramatically speed up the policy rollout and evaluation process, however, there will be a tradeoff in accuracy of the dc simulation compared to the full dynamic simulation approach of this work.

BIBLIOGRAPHY

1. M. Patel and et. al., "Real-time application of sychrophasors for improving reliability," tech. rep., North American Electric Reliability Corporation, Princeton, New Jersey, October 2010.

2. PowerWorld Corporation, 2001 South First Street, Champaign, IL 61820, *PowerWorld Corporation SimManual Verison 17 User's Guide*.

3. "Ieee 10 generator 39 bus system." Electronic. http://sys.elec.kitami-it.ac.jp/ueda/demo/WebPF/39-New-England.pdf.

4. "The president's climate action plan," tech. rep., The Executive Office of the President, June 2013.

5. N. Miller and Z. Ye, "Report on distributed generation penetration study," tech. rep., National Renewable Energy Laboratory, August 2003.

6. "Economic benefits of increasing electric grid resilience to weather outages," tech. rep., United States Executive Office of the President, August 2013.

7. P. Barber, T. Boston, M. Fidrych, S. Jones, Y. Mansour, D. McMaster, B. Newman, and T. Winter, "Technical analysis of the august 14, 2003 blackout," tech. rep., North American Electric Reliability Council, July 2004.

8. N. Lu, T. Taylor, W. Jiang, C. Jin, J. Correia, L. Leung, and P. C. Wong, "Climate change impacts on residential and commercial loads in the western u.s. grid," *IEEE Transactions on Power Systems*, vol. 25, pp. 480–488, Feb 2010.

9. Z. Darabi and M. Ferdowsi, "Aggregated impact of plug-in hybrid electric vehicles on electricity demand profile," *IEEE Transactions on Sustainable Energy*, vol. 2, pp. 501–508, Oct 2011.

10. R. Meier, E. Cotilla-Sanchez, B. McCamish, D. Chiu, M. Histand, J. Landford, and R. Bass, "Power system data management and analysis using synchrophasor data," in *2014 IEEE Conference on Technologies for Sustainability (SusTech)*, pp. 225–231, July 2014.

11. B. McCamish, M. Histand, J. Landford, R. Bass, D. Chiu, R. Meier, and E. Cotilla-Sanchez, "Managing pmu data sets with bitmap indexes," in *2014 IEEE Conference on Technologies for Sustainability (SusTech)*, pp. 219–224, July 2014.

12. R. Meier, E. Cotilla-Sanchez, and A. Fern, "A policy switching approach to consolidating load shedding and islanding protection schemes," in *Power Systems Computation Conference (PSCC), 2014*, pp. 1–7, Aug 2014.

13. S. Horowitz, A. Phadke, and B. Renz, “The future of power transmission,” *IEEE Power and Energy Magazine*, vol. 8, no. 2, pp. 34–40, 2010.

14. M. R. Starke, D. T. Rizy, and Y. M. A., “Synchrophasor technologies and their deployment in the recovery act smart grid programs,” tech. rep., US Department of Energy, August 2013.

15. K. Stewart, “Increasing network visibility: Western interconnection synchrophasor program (wisp) sgig infrastructure deployment,” presentation, Western Electricity Coordinating Council, February 2013.

16. S. Das and T. Sidhu, “Detecting synchrophasors computed over fault/switching transients,” *IET Generation, Transmission & Distribution*, April 2014.

17. G. Barchi, D. Macii, D. Belega, and D. Petri, “Performance of synchrophasor estimators in transient conditions: A comparative analysis,” *IEEE Transactions on Instrumentation and Measurement*, vol. 62, pp. 2410–2418, Sept 2013.

18. M. Wang, J. H. Chow, P. Gao, X. T. Jiang, Y. Xia, S. G. Ghiocel, B. Fardanesh, G. Stefopolous, Y. Kokai, N. Saito, and M. Razanousky, “A low-rank matrix approach for the analysis of large amounts of power system synchrophasor data,” in *48th Hawaii International Conference on System Sciences (HICSS), 2015*, pp. 2637–2644, Jan 2015.

19. D. Batz, E. Goff, D. Maughan, J. Brenton, B. Harrell, L. Kaiser, D. Dunn, C. Hawk, D. Norton, G. Williams, M. Henrie, P. Clark, H. Kenchington, and S. Elwart, “Roadmap to achieve energy delivery systems cybersecurity,” tech. rep., Energy Sector Control Systems Working Group, September 2011.

20. J. Chow, A. Chakrabortty, M. Arcak, B. Bhargava, and A. Salazar, “Synchronized phasor data based energy function analysis of dominant power transfer paths in large power systems,” *IEEE Transactions on Power Systems*, vol. 22, pp. 727–734, May 2007.

21. T.-C. Lin, P.-Y. Lin, and C.-W. Liu, “An algorithm for locating faults in three-terminal multisection nonhomogeneous transmission lines using synchrophasor measurements,” *IEEE Transactions on Smart Grid*, vol. 5, pp. 38–50, Jan 2014.

22. J. Ma, P. Zhang, H. jun Fu, B. Bo, and Z.-Y. Dong, “Application of phasor measurement unit on locating disturbance source for low-frequency oscillation,” *IEEE Transactions on Smart Grid*, vol. 1, pp. 340–346, Dec 2010.

23. E. Cotilla-Sanchez, P. Hines, and C. Danforth, “Predicting critical transitions from time series synchrophasor data,” *IEEE Transactions on Smart Grid*, vol. 3, pp. 1832–1840, Dec 2012.

24. P. Ashton, G. Taylor, M. Irving, I. Pisica, A. Carter, and M. Bradley, "Novel application of detrended fluctuation analysis for state estimation using synchrophasor measurements," *IEEE Transactions on Power Systems*, vol. 28, pp. 1930–1938, May 2013.

25. S. Dowi and G. Li, "Influence of phasor measurement unit in power system dynamic state estimation," in *2nd International Symposium on Instrumentation and Measurement, Sensor Network and Automation (IMSNA), 2013*, pp. 395–399, Dec 2013.

26. A. G. Phadke and J. S. Thorp, *Synchronized phasor measurements and their applications.* Springer, 2008.

27. A. Phadke, J. Thorp, R. Nuqui, and M. Zhou, "Recent developments in state estimation with phasor measurements," in *IEEE/PES Power Systems Conference and Exposition, 2009. PSCE '09*, pp. 1–7, March 2009.

28. S. Pahwa, C. Scoglio, S. Das, and N. Schulz, "Load-shedding strategies for preventing cascading failures in power grid," *Electric Power Components and Systems*, vol. 41, pp. 879–895, 2013.

29. L. Hajdu, J. Peschon, W. F. Tinney, and D. Piercy, "Optimum load-shedding policy for power systems," *IEEE Transactions on Power Apparatus and Systems*, vol. PAS-87, no. 3, pp. 784–795, 1968.

30. M. Ahsan, A. Chowdhury, S. Ahmed, I. Bhuyan, M. Haque, and H. Rahman, "Technique to develop auto load shedding and islanding scheme to prevent power system blackout," *IEEE Transactions on Power Systems*, vol. 27, no. 1, pp. 198–205, 2012.

31. R. Faranda, A. Pievatolo, and E. Tironi, "Load shedding: A new proposal," *IEEE Transactions on Power Systems*, vol. 22, no. 4, pp. 2086–2093, 2007.

32. H. Bevrani, A. G. Tikdari, and T. Hiyama, "An intelligent based power system load shedding design using voltage and frequency information," in *The 2010 International Conference on Modelling, Identification and Control (ICMIC)*, pp. 545–549, 2010.

33. H. Dola and B. Chowdhury, "Intentional islanding and adaptive load shedding to avoid cascading outages," in *IEEE Power Engineering Society General Meeting, 2006*, pp. 8 pp.–, 2006.

34. B. Yang, V. Vittal, and G. Heydt, "Slow-coherency-based controlled islanding - a demonstration of the approach on the august 14, 2003 blackout scenario," *IEEE Transactions on Power Systems*, vol. 21, no. 4, pp. 1840–1847, 2006.

35. S. Wang, Z. Li, L. Wu, M. Shahidehpour, and Z. Li, "New metrics for assessing the reliability and economics of microgrids in distribution system," *IEEE Transactions on Power Systems*, vol. 28, no. 3, pp. 2852–2861, 2013.

36. J. Li, C.-C. Liu, and K. Schneider, "Controlled partitioning of a power network considering real and reactive power balance," *IEEE Transactions on Smart Grid*, vol. 1, no. 3, pp. 261–269, 2010.

37. S. Amin and B. Wollenberg, "Toward a smart grid: power delivery for the 21st century," *IEEE Power and Energy Magazine*, vol. 3, no. 5, pp. 34–41, 2005.

38. M. Rahnamay-Naeini, Z. Wang, A. Mammoli, and M. Hayat, "Impacts of control and communication system vulnerabilities on power systems under contingencies," in *IEEE Power and Energy Society General Meeting, 2012*, pp. 1–7, 2012.

39. Y. Zhao, N. Zhou, J. Zhou, K. Xie, Y. Liu, and J. Kuang, "A heuristic approach to local load shedding scheme for reliability assessment of bulk power systems," in *IEEE/PES Transmission and Distribution Conference and Exhibition: Asia and Pacific, 2005*, pp. 1–5, 2005.

40. H. Seyedi and M. Sanaye-Pasand, "New centralised adaptive load-shedding algorithms to mitigate power system blackouts," *Generation, Transmission Distribution, IET*, vol. 3, no. 1, pp. 99–114, 2009.

41. E. Cotilla-Sanchez, P. Hines, C. Barrows, S. Blumsack, and M. Patel, "Multi-attribute partitioning of power networks based on electrical distance," *IEEE Transactions on Power Systems*, vol. 28, no. 4, pp. 4978–4987, 2013.

42. M. Hanley, "Frequency instability problems in north american interconnections," tech. rep., National Energy Technology Laboratory, 2011.

43. C. Liu, K. Sun, Z. Rather, Z. Chen, C. Bak, P. Thogersen, and P. Lund, "A systematic approach for dynamic security assessment and the corresponding preventive control scheme based on decision trees," *IEEE Transactions on Power Systems*, vol. PP, no. 99, pp. 1–14, 2013.

44. M. Falahi, K. Butler-Purry, and M. Ehsani, "Dynamic reactive power control of islanded microgrids," *IEEE Transactions on Power Systems*, vol. 28, no. 4, pp. 3649–3657, 2013.

45. B. Stott, J. Jardim, and O. Alsac, "Dc power flow revisited," *IEEE Transactions on Power Systems*, vol. 24, no. 3, pp. 1290–1300, 2009.

46. D. Xu and A. Girgis, "Optimal load shedding strategy in power systems with distributed generation," in *IEEE Power Engineering Society Winter Meeting, 2001.*, vol. 2, pp. 788–793 vol.2, 2001.

47. B. King, A. Fern, and J. Hostetler, "On adversarial policy switching with experiments in real-time strategy games," 2013.

48. "Ieee standard for synchrophasor data transfer for power systems," *IEEE Std C37.118.2-2011 (Revision of IEEE Std C37.118-2005)*, pp. 1–53, Dec 2011.

49. "Ieee standard for synchrophasor measurements for power systems," *IEEE Std C37.118.1-2011 (Revision of IEEE Std C37.118-2005)*, pp. 1–61, Dec 2011.

50. J. D. Glover, M. Sarma, and T. Overbye, *Power System Analysis and Design Fifth Edition*. Cengage Learning, fifth ed., 2012.

51. P. Kundur, *Power System Stability and Control*. McGraw-Hill Inc., 1994.

52. Siemens Power Technologies International, 400 State Street Schenectady, NY 12301, *Siemens PSS/e 33.4 Program Operation Manual*.

53. Siemens Power Technologies International, 400 State Street Schenectady, NY 12301, *Siemens PSS/e 33.4 Models Library*.

54. P. Cuffe and A. Keane, "Visualizing the electrical structure of power systems," *IEEE Systems Journal*, vol. PP, no. 99, pp. 1–12, 2015.

55. S. J. Russell and P. Norvig, *Artificial Intelligence: A Modern Approach*. Pearson Education, 2010.

56. M. L. Puterman, *Markov decision processes: discrete stochastic dynamic programming*, vol. 414. 2009.

57. T. Bylander, "The computational complexity of propositional strips planning," *Artificial Intelligence*, vol. 69, no. 1, pp. 165–204, 1994.

58. D. H. Johnson, "Signal-to-noise ratio," *Scholarpedia*, vol. 1, no. 12, p. 2088, 2006. revision #91770.

59. J. Runge, "On the graph-theoretical interpretation of pearson correlations in a multivariate process and a novel partial correlation measure," pp. 1–20, Oct 2013.

60. D. Skillicorn, "Outlier detection using semantic sensors," in *IEEE International Conference on Intelligence and Security Informatics (ISI), 2012*, pp. 42–47, 2012.

61. R. Zimmerman, C. Murillo-Snchez, and R. Thomas, "Matpower: Steady-state operations, planning, and analysis tools for power systems research and education," *Power Systems, IEEE Transactions on*, vol. 26, pp. 12–19, Feb 2011.

62. J. Song, E. Cotilla-Sanchez, G. Ghanavati, and P. D. H. Hines, "Dynamic modeling of cascading failure in power systems." Journal Submitted to IEEE Transactions on Power Systems – Preprint at ArXiv.org, 2015.

63. H. S. Chang, R. Givan, and E. K. Chong, "Parallel rollout for online solution of partially observable markov decision processes," *Discrete Event Dynamic Systems*, vol. 14, no. 3, pp. 309–341, 2004.

64. M. Kearns, Y. Mansour, and A. Y. Ng, "A sparse sampling algorithm for near-optimal planning in large markov decision processes," *Machine Learning*, vol. 49, no. 2-3, pp. 193–208, 2002.

APPENDICES

A APPENDIX Dynamic Model Parameters

9-Bus Machine Parameters: 'GENSAL' Model			
Parameter	Bus 1	Bus 2	Bus 3
H	23.64	6.4	3.01
D	23.64	6.4	3.01
X_d	0.146	0.8958	1.3125
X_q	0.0969	0.8645	1.2578
X'_d	0.0608	0.1198	0.1813
X''_d	0.05	0.05	0.05
X_l	0	0	0
T'_{do}	8.96	6	5.89
T''_{do}	0.0001	0.0001	0.0001
T''_{qo}	0.0001	0.0001	0.0001
S(1.0)	0	0	0
S(1.2)	0	0	0

9-Bus Governor and Exciter Model Parameters†			
'TGOV1'		'SEXS_PTI'	
Parameter	Value	Parameter	Value
Trate	0	T_a/T_b	0.1
R	0.05	T_b	10
T_1	2	K	100
V_{MAX}	1	T_e	0.1
V_{MIN}	0	EFD_{min}	-5
T_2	0	EFD_{max}	5
T_3	1	-	-
Dt	0	-	-

†Identical governors and exciters used for all machines.

39-Bus Machine Parameters: 'GENROU' Model			
Machine Specific		General	
BUS	H	Parameter	Value
30	42	T'_{do}	5
31	30.3	T''_{do}	0.05
32	35.8	T'_{qo}	1.5
33	28.6	T''_{qo}	0.05
34	26	X_d	0.6
35	34.8	X_q	0.55
36	26.4	X'_d	0.075
37	24.3	X'_q	0.1125
38	34.5	$X''_d = X''_q$	0.05
39	50	X_l	0.001
-	-	S(1.0)	0.11
-	-	S(1.2)	0.48
-	-	D	1

39-Bus Governor and Exciter Model Parameters†			
'IEEEG2'		'IEEET1'	
Parameter	Value	Parameter	Value
K	20	T_R	0.1
T_1	50	K_A	100
T_2	9.99	T_A	0.02
T_3	1	V_{RMAX}	*
P_{MAX}	20	V_{RMIN}	0
P_{MIN}	0	K_E	*
T_4	1	T_E	0.1
-	-	K_F	0.03
-	-	T_F	1
-	-	Switch	0
-	-	E_1	2.9
-	-	$S_E E_1$	0.5
-	-	E_2	3.9
-	-	$S_E E_2$	0.86

†Identical governors and exciters used for all machines.

* Denotes PSS/E automatically determines this value.

2383-Bus Poland Governor Model Parameters†	
'IEEEG2'	
Parameter	Value
K	20
T_1	50
T_2	9.99
T_3	1
P_{MAX}	100
P_{MIN}	-100
T_4	1

†Identical governors used for all machines.

2383-Bus Poland Model Parameters								
'GENROU'					'IEEET1'			
Machine Specific			General		Machine Specific		General	
Bus	H	D	Parameter	Value	Bus	T_e	Parameter	Value
10	13.64	5.07	T'_{do}	5	10	0.10264	T_R	0.1
16	20.55	7.94	T''_{do}	0.05	16	0.11687	K_A	100
17	28.32	11.06	T'_{qo}	1	17	0.11269	T_A	0.02
18	75.00	31.20	T''_{qo}	0.05	18	0.09817	V_{RMAX}	*
29	12.38	4.55	X_d	0.7	29	0.10690	V_{RMIN}	*
30	19.75	7.58	X_q	0.6	30	0.08590	K_E	*
31	26.60	10.35	X'_d	0.075	31	0.08841	K_F	0.03
41	9.32	3.28	X'_q	0.09	41	0.11963	T_F	1
42	12.56	4.72	$X''_d = X''_q$	0.05	42	0.11069	Switch	0
43	13.85	5.29	X_l	0	43	0.10100	E_1	2.9
44	13.85	4.89	S(1.0)	0	44	0.11062	$S_E E_1$	0.5
45	5.91	1.88	S(1.2)	0	45	0.10504	E_2	3.9
63	19.04	7.13	-	-	63	0.11163	$S_E E_2$	0.86
64	14.72	5.18	-	-	64	0.11702	-	-
67	21.20	8.41	-	-	67	0.11084	-	-
83	9.86	3.54	-	-	83	0.10083	-	-
84	9.86	3.23	-	-	84	0.09850	-	-
85	7.59	2.19	-	-	85	0.09469	-	-
86	7.59	2.31	-	-	86	0.08317	-	-
93	7.59	2.37	-	-	93	0.09726	-	-

95	7.38	2.17	-	-	95	0.08822	-	-
97	6.89	2.03	-	-	97	0.09283	-	-
103	12.38	4.58	-	-	103	0.08716	-	-
104	9.86	3.36	-	-	104	0.08905	-	-
105	14.29	5.40	-	-	105	0.11720	-	-
109	10.40	3.81	-	-	109	0.11271	-	-
110	10.40	3.48	-	-	110	0.11070	-	-
111	12.77	4.38	-	-	111	0.10050	-	-
123	7.03	2.26	-	-	123	0.10405	-	-
124	7.70	2.23	-	-	124	0.11654	-	-
125	20.86	8.16	-	-	125	0.10274	-	-
127	19.90	7.86	-	-	127	0.08009	-	-
131	24.54	9.41	-	-	131	0.09005	-	-
132	16.06	5.96	-	-	132	0.10168	-	-
139	16.06	6.16	-	-	139	0.11238	-	-
140	9.32	2.92	-	-	140	0.11835	-	-
176	17.96	6.94	-	-	176	0.11311	-	-
177	9.32	3.24	-	-	177	0.11032	-	-
180	5.00	1.34	-	-	180	0.08108	-	-
181	8.85	2.72	-	-	181	0.09229	-	-
182	11.77	3.92	-	-	182	0.10593	-	-
184	5.00	1.33	-	-	184	0.10885	-	-
185	5.00	1.13	-	-	185	0.08737	-	-
186	5.00	1.49	-	-	186	0.08308	-	-
192	7.05	2.15	-	-	192	0.09528	-	-
196	5.02	1.04	-	-	196	0.09829	-	-

198	5.02	1.36	-	-	198	0.09008	-	-
205	5.32	1.45	-	-	205	0.09899	-	-
213	5.24	1.55	-	-	213	0.10259	-	-
264	5.05	1.10	-	-	264	0.10455	-	-
269	5.13	1.36	-	-	269	0.09490	-	-
277	6.51	1.81	-	-	277	0.09674	-	-
278	6.30	1.94	-	-	278	0.09026	-	-
279	6.30	1.63	-	-	279	0.10404	-	-
281	7.59	2.58	-	-	281	0.11362	-	-
282	5.86	1.62	-	-	282	0.11168	-	-
289	5.05	1.44	-	-	289	0.10275	-	-
294	5.04	1.13	-	-	294	0.11501	-	-
314	5.03	1.07	-	-	314	0.08303	-	-
328	5.95	1.74	-	-	328	0.08004	-	-
329	5.95	1.70	-	-	329	0.10619	-	-
330	5.95	1.85	-	-	330	0.10313	-	-
331	5.93	1.90	-	-	331	0.08403	-	-
334	5.03	1.15	-	-	334	0.11809	-	-
346	9.32	3.22	-	-	346	0.10172	-	-
347	5.22	1.24	-	-	347	0.11430	-	-
359	5.03	1.38	-	-	359	0.11499	-	-
365	5.11	1.29	-	-	365	0.08823	-	-
382	5.17	1.51	-	-	382	0.09270	-	-
383	5.17	1.16	-	-	383	0.08892	-	-
385	5.13	1.54	-	-	385	0.09926	-	-
390	5.10	1.07	-	-	390	0.09315	-	-

395	5.22	1.44	-	-	395	0.09011	-	-
404	5.06	1.35	-	-	404	0.08508	-	-
426	5.07	1.05	-	-	426	0.10760	-	-
444	5.02	1.11	-	-	444	0.09394	-	-
451	5.10	1.21	-	-	451	0.09137	-	-
482	5.02	1.39	-	-	482	0.08796	-	-
492	5.04	1.20	-	-	492	0.09019	-	-
493	10.05	3.43	-	-	493	0.09182	-	-
494	10.05	3.34	-	-	494	0.10567	-	-
514	7.48	2.32	-	-	514	0.08839	-	-
515	7.48	2.20	-	-	515	0.11694	-	-
525	5.13	1.48	-	-	525	0.10300	-	-
536	5.13	1.37	-	-	536	0.10720	-	-
537	5.08	1.18	-	-	537	0.11976	-	-
556	5.06	1.41	-	-	556	0.10568	-	-
580	5.03	1.46	-	-	580	0.11125	-	-
584	5.06	1.39	-	-	584	0.10419	-	-
585	5.09	1.46	-	-	585	0.09960	-	-
607	5.02	1.42	-	-	607	0.10652	-	-
612	8.69	3.01	-	-	612	0.08654	-	-
613	9.32	3.04	-	-	613	0.09281	-	-
615	5.03	1.32	-	-	615	0.08553	-	-
623	5.16	1.28	-	-	623	0.09566	-	-
639	5.21	1.21	-	-	639	0.09549	-	-
651	5.10	1.07	-	-	651	0.09328	-	-
654	5.03	1.42	-	-	654	0.09355	-	-

664	5.13	1.25	-	-	664	0.10230	-	-
670	5.06	1.51	-	-	670	0.09787	-	-
674	5.02	1.20	-	-	674	0.08559	-	-
688	8.72	2.91	-	-	688	0.11905	-	-
692	5.03	1.23	-	-	692	0.10390	-	-
699	5.08	1.05	-	-	699	0.10158	-	-
712	5.03	1.13	-	-	712	0.09211	-	-
730	5.15	1.45	-	-	730	0.10534	-	-
732	5.02	1.10	-	-	732	0.09448	-	-
735	5.09	1.25	-	-	735	0.08096	-	-
740	5.09	1.33	-	-	740	0.09538	-	-
744	7.89	2.70	-	-	744	0.09701	-	-
754	6.73	1.99	-	-	754	0.11112	-	-
755	9.61	3.19	-	-	755	0.09981	-	-
760	5.07	1.04	-	-	760	0.08571	-	-
766	5.05	1.13	-	-	766	0.11520	-	-
784	5.02	1.10	-	-	784	0.08751	-	-
790	6.08	1.58	-	-	790	0.09395	-	-
795	5.04	1.42	-	-	795	0.11178	-	-
798	5.06	1.29	-	-	798	0.11082	-	-
814	5.97	1.60	-	-	814	0.10852	-	-
834	6.19	1.74	-	-	834	0.10068	-	-
878	5.06	1.33	-	-	878	0.10178	-	-
884	5.05	1.30	-	-	884	0.09793	-	-
892	5.69	1.31	-	-	892	0.09269	-	-
895	5.19	1.28	-	-	895	0.09751	-	-

901	5.08	1.08	-	-	901	0.09923	-	-
910	5.10	1.28	-	-	910	0.11206	-	-
911	12.99	4.85	-	-	911	0.08928	-	-
912	12.99	4.85	-	-	912	0.10465	-	-
914	5.34	1.33	-	-	914	0.08584	-	-
917	5.05	1.38	-	-	917	0.11075	-	-
919	5.47	1.21	-	-	919	0.09929	-	-
920	5.04	1.40	-	-	920	0.10962	-	-
929	6.38	1.96	-	-	929	0.11221	-	-
959	5.05	1.45	-	-	959	0.09773	-	-
968	5.02	1.23	-	-	968	0.11090	-	-
993	5.09	1.51	-	-	993	0.09020	-	-
994	5.04	1.34	-	-	994	0.08583	-	-
995	6.84	2.04	-	-	995	0.10163	-	-
996	5.92	1.49	-	-	996	0.08587	-	-
997	5.92	1.78	-	-	997	0.11257	-	-
1004	5.09	1.23	-	-	1004	0.10505	-	-
1024	5.01	1.11	-	-	1024	0.10543	-	-
1027	5.54	1.39	-	-	1027	0.09463	-	-
1028	5.06	1.13	-	-	1028	0.11866	-	-
1029	5.54	1.44	-	-	1029	0.08118	-	-
1053	6.29	1.62	-	-	1053	0.10768	-	-
1054	5.65	1.68	-	-	1054	0.10865	-	-
1105	5.17	1.39	-	-	1105	0.09910	-	-
1106	5.49	1.55	-	-	1106	0.09102	-	-
1107	5.23	1.10	-	-	1107	0.09282	-	-

1138	5.97	1.78	-	-	1138	0.10251	-	-
1140	9.97	3.51	-	-	1140	0.09658	-	-
1141	9.15	2.86	-	-	1141	0.09277	-	-
1175	5.82	1.83	-	-	1175	0.08614	-	-
1182	7.21	2.35	-	-	1182	0.11030	-	-
1183	7.59	2.40	-	-	1183	0.09694	-	-
1184	7.59	2.13	-	-	1184	0.10155	-	-
1191	7.30	2.16	-	-	1191	0.08260	-	-
1192	10.40	3.50	-	-	1192	0.09843	-	-
1201	7.15	2.36	-	-	1201	0.10559	-	-
1202	7.15	1.98	-	-	1202	0.10351	-	-
1203	7.15	2.02	-	-	1203	0.08020	-	-
1232	6.12	1.96	-	-	1232	0.09747	-	-
1233	5.32	1.40	-	-	1233	0.09361	-	-
1244	5.41	1.42	-	-	1244	0.09028	-	-
1247	5.34	1.27	-	-	1247	0.10123	-	-
1250	9.26	3.29	-	-	1250	0.10084	-	-
1268	5.01	1.04	-	-	1268	0.11867	-	-
1316	5.02	1.08	-	-	1316	0.11302	-	-
1325	5.03	1.13	-	-	1325	0.08744	-	-
1349	5.03	1.05	-	-	1349	0.09024	-	-
1356	5.02	1.44	-	-	1356	0.09677	-	-
1359	5.02	1.30	-	-	1359	0.08081	-	-
1393	5.28	1.57	-	-	1393	0.08190	-	-
1403	5.09	1.29	-	-	1403	0.08718	-	-
1416	13.01	4.82	-	-	1416	0.11545	-	-

1417	7.59	2.17	-	-	1417	0.10212	-	-
1418	5.43	1.49	-	-	1418	0.09731	-	-
1426	15.69	6.04	-	-	1426	0.09314	-	-
1429	5.00	1.26	-	-	1429	0.11631	-	-
1469	5.01	1.24	-	-	1469	0.11663	-	-
1475	5.05	1.38	-	-	1475	0.09187	-	-
1504	5.67	1.31	-	-	1504	0.11448	-	-
1505	6.05	1.81	-	-	1505	0.10711	-	-
1514	5.05	1.17	-	-	1514	0.08370	-	-
1534	5.01	1.25	-	-	1534	0.08491	-	-
1536	9.15	3.21	-	-	1536	0.10197	-	-
1537	9.86	3.18	-	-	1537	0.09564	-	-
1538	9.64	3.31	-	-	1538	0.09663	-	-
1542	5.19	1.32	-	-	1542	0.11414	-	-
1543	5.03	1.40	-	-	1543	0.10498	-	-
1550	5.04	1.30	-	-	1550	0.08030	-	-
1566	6.18	1.65	-	-	1566	0.08465	-	-
1587	6.38	1.68	-	-	1587	0.11838	-	-
1600	5.38	1.42	-	-	1600	0.10766	-	-
1602	7.59	2.44	-	-	1602	0.11544	-	-
1603	7.59	2.47	-	-	1603	0.11467	-	-
1609	5.01	1.19	-	-	1609	0.08172	-	-
1617	5.04	1.15	-	-	1617	0.08014	-	-
1620	5.03	1.15	-	-	1620	0.11058	-	-
1627	5.03	1.46	-	-	1627	0.10521	-	-
1630	5.01	1.45	-	-	1630	0.09216	-	-

1635	5.01	1.03	-	-	1635	0.11637	-	-
1638	5.65	1.58	-	-	1638	0.08198	-	-
1664	8.24	2.65	-	-	1664	0.11999	-	-
1669	6.10	1.56	-	-	1669	0.08205	-	-
1673	6.08	1.69	-	-	1673	0.08244	-	-
1674	6.94	1.93	-	-	1674	0.10876	-	-
1679	5.06	1.37	-	-	1679	0.09546	-	-
1683	5.05	1.11	-	-	1683	0.11629	-	-
1685	5.07	1.28	-	-	1685	0.09758	-	-
1686	6.08	1.72	-	-	1686	0.09615	-	-
1698	5.06	1.24	-	-	1698	0.11866	-	-
1700	5.01	1.25	-	-	1700	0.09019	-	-
1706	5.32	1.60	-	-	1706	0.10731	-	-
1710	5.06	1.48	-	-	1710	0.10547	-	-
1712	7.38	2.13	-	-	1712	0.09056	-	-
1717	5.05	1.25	-	-	1717	0.11279	-	-
1719	5.04	1.36	-	-	1719	0.08619	-	-
1726	5.08	1.45	-	-	1726	0.09917	-	-
1728	5.06	1.49	-	-	1728	0.11067	-	-
1730	5.03	1.03	-	-	1730	0.09088	-	-
1734	5.02	1.34	-	-	1734	0.10549	-	-
1735	5.11	1.17	-	-	1735	0.08261	-	-
1739	5.06	1.52	-	-	1739	0.11803	-	-
1742	5.01	1.48	-	-	1742	0.11600	-	-
1749	5.13	1.40	-	-	1749	0.11768	-	-
1758	5.04	1.25	-	-	1758	0.11839	-	-

1760	6.19	1.90	-	-	1760	0.08950	-	-
1761	6.68	1.94	-	-	1761	0.11629	-	-
1763	6.08	1.53	-	-	1763	0.10714	-	-
1764	5.92	1.40	-	-	1764	0.10753	-	-
1768	5.09	1.41	-	-	1768	0.10922	-	-
1788	5.07	1.52	-	-	1788	0.11513	-	-
1793	5.06	1.13	-	-	1793	0.10515	-	-
1799	5.03	1.49	-	-	1799	0.08781	-	-
1807	5.06	1.25	-	-	1807	0.10866	-	-
1844	5.03	1.23	-	-	1844	0.10987	-	-
1845	5.03	1.25	-	-	1845	0.08825	-	-
1870	5.03	1.10	-	-	1870	0.11932	-	-
1871	5.01	1.27	-	-	1871	0.09166	-	-
1874	5.09	1.30	-	-	1874	0.09219	-	-
1875	5.01	1.47	-	-	1875	0.11638	-	-
1882	9.32	3.30	-	-	1882	0.08781	-	-
1883	9.32	3.00	-	-	1883	0.11510	-	-
1894	5.03	1.16	-	-	1894	0.09949	-	-
1895	5.01	1.08	-	-	1895	0.09950	-	-
1904	5.37	1.32	-	-	1904	0.09482	-	-
1918	5.13	1.11	-	-	1918	0.09513	-	-
1921	6.09	1.82	-	-	1921	0.11757	-	-
1932	5.05	1.30	-	-	1932	0.08237	-	-
1940	5.04	1.14	-	-	1940	0.09435	-	-
1947	5.13	1.52	-	-	1947	0.08769	-	-
1960	5.03	1.36	-	-	1960	0.08392	-	-

1961	5.01	1.22	-	-	1961	0.09320	-	-
1962	5.01	1.41	-	-	1962	0.09131	-	-
1964	5.01	1.08	-	-	1964	0.11784	-	-
1966	5.06	1.23	-	-	1966	0.10138	-	-
1970	5.04	1.04	-	-	1970	0.10341	-	-
1974	5.08	1.16	-	-	1974	0.08162	-	-
1976	5.06	1.04	-	-	1976	0.08381	-	-
1977	5.06	1.39	-	-	1977	0.11508	-	-
1993	5.06	1.50	-	-	1993	0.09403	-	-
1995	5.45	1.23	-	-	1995	0.11026	-	-
1996	5.00	1.03	-	-	1996	0.11077	-	-
1998	5.01	1.19	-	-	1998	0.09863	-	-
2010	9.32	3.01	-	-	2010	0.08772	-	-
2021	6.80	1.82	-	-	2021	0.10172	-	-
2022	6.75	2.06	-	-	2022	0.09742	-	-
2026	5.54	1.41	-	-	2026	0.11260	-	-
2027	5.26	1.16	-	-	2027	0.10055	-	-
2033	5.12	1.55	-	-	2033	0.10859	-	-
2034	5.01	1.28	-	-	2034	0.09367	-	-
2036	5.01	1.46	-	-	2036	0.11829	-	-
2046	5.02	1.06	-	-	2046	0.09239	-	-
2085	5.01	1.40	-	-	2085	0.10423	-	-
2088	5.01	1.04	-	-	2088	0.11110	-	-
2099	5.39	1.40	-	-	2099	0.11169	-	-
2106	5.02	1.47	-	-	2106	0.08303	-	-
2107	5.06	1.41	-	-	2107	0.08657	-	-

2108	5.01	1.20	-	-	2108	0.09228	-	-
2115	5.05	1.06	-	-	2115	0.11158	-	-
2119	7.38	2.17	-	-	2119	0.10369	-	-
2121	5.02	1.37	-	-	2121	0.11260	-	-
2127	5.05	1.22	-	-	2127	0.08831	-	-
2138	6.08	1.88	-	-	2138	0.10975	-	-
2139	5.86	1.82	-	-	2139	0.10738	-	-
2140	5.17	1.25	-	-	2140	0.11583	-	-
2153	5.02	1.17	-	-	2153	0.11498	-	-
2159	5.26	1.54	-	-	2159	0.09688	-	-
2164	5.09	1.25	-	-	2164	0.10194	-	-
2167	6.94	2.07	-	-	2167	0.10501	-	-
2168	6.08	1.90	-	-	2168	0.09140	-	-
2171	5.14	1.17	-	-	2171	0.11615	-	-
2194	5.22	1.54	-	-	2194	0.09373	-	-
2197	5.58	1.40	-	-	2197	0.09734	-	-
2204	5.56	1.49	-	-	2204	0.09625	-	-
2213	5.06	1.30	-	-	2213	0.09176	-	-
2217	5.09	1.52	-	-	2217	0.10745	-	-
2218	5.03	1.29	-	-	2218	0.10351	-	-
2221	6.06	1.65	-	-	2221	0.09136	-	-
2225	5.03	1.03	-	-	2225	0.10375	-	-
2234	5.06	1.04	-	-	2234	0.11333	-	-
2237	5.36	1.52	-	-	2237	0.08791	-	-
2248	5.04	1.32	-	-	2248	0.09093	-	-
2268	5.04	1.19	-	-	2268	0.10765	-	-

2271	5.05	1.34	-	-	2271	0.08777	-	-
2272	5.22	1.57	-	-	2272	0.09166	-	-
2273	5.14	1.24	-	-	2273	0.10807	-	-
2278	5.03	1.05	-	-	2278	0.11314	-	-
2290	5.00	1.36	-	-	2290	0.08054	-	-
2293	5.07	1.19	-	-	2293	0.09552	-	-
2294	5.02	1.48	-	-	2294	0.10682	-	-
2296	5.29	1.38	-	-	2296	0.09713	-	-
2298	5.01	1.07	-	-	2298	0.11538	-	-
2307	5.01	1.13	-	-	2307	0.10981	-	-
2323	5.02	1.35	-	-	2323	0.11003	-	-
2328	5.06	1.37	-	-	2328	0.08018	-	-
2330	5.01	1.18	-	-	2330	0.11303	-	-
2336	6.19	1.69	-	-	2336	0.08525	-	-
2339	5.37	1.60	-	-	2339	0.08675	-	-
2361	6.10	1.96	-	-	2361	0.09740	-	-
2372	5.80	1.80	-	-	2372	0.08267	-	-
2376	5.04	1.38	-	-	2376	0.10554	-	-
2379	5.15	1.16	-	-	2379	0.10212	-	-
2380	6.08	1.51	-	-	2380	0.09555	-	-
2381	6.08	1.56	-	-	2381	0.11596	-	-

* Denotes PSS/E automatically determines this value.